From NMR Spectra to Structure

JULIO C. FACELLI,[1,2] MARTA B. FERRARO[3]

[1]*Center for High Performance Computing, The University of Utah, Salt Lake City, UT 84112-5775*
[2]*Department of Biomedical Informatics, The University of Utah, Salt Lake City, UT 84112-5775*
[3]*Departamento de Física and IFIBA (CONICET), Facultad de Ciencias Exactas y Naturales, Universidad de Buenos Aires, Ciudad Universitaria, Buenos Aires, Argentina*

ABSTRACT: This article discusses the existing methods to correlate NMR parameters describing the high resolution NMR spectra of liquids and solid systems with their structural parameters. Those methods are divided into direct and indirect ones. This article includes two types of direct methods: those based on the Nuclear Overhauser Effect (NOE) contributions to the NMR relaxation and those based on direct measurements of the dipolar couplings using several experimental approaches. Indirect methods are based on the intrinsic dependence of J couplings and shieldings on the atomic coordinates of the atoms in a molecule and its surroundings, requiring complex quantum mechanical calculations to relate NMR spectral properties to molecular and crystal structure. This article discusses how changes in chemical bonding, conformation, and stereo configurations that cause measurable changes in NMR parameters closely related to molecular and crystal structure. The final section provides information about the software and hardware required to perform calculations needed to solve structural problems using high resolution NMR. This article intends to provide molecular structural researchers new to the field of NMR, with an overall panorama of the potential of using high resolution NMR for structure elucidation, when other more traditional techniques are not feasible. To this end and to emphasize the didactic value of this work, after each section a brief conclusion has been added to recap the critical concepts. Concepts Magn Reson Part A 42A: 261–289, 2013.

KEY WORDS: high resolution NMR; molecular structure; crystal structure; solid state NMR; chemical shifts; J couplings

INTRODUCTION

This article presents a description on how the parameters defining the high resolution NMR spectra of liquids and solids, chemical shifts, *J* couplings, and direct dipolar couplings can be used to extract structural information, such as connectivity, coordination, symmetry, conformation, and molecular geometry. This article presents the theoretical background that establishes the relationship between spectral parameters and molecular structure, the tools available to obtain this information, and selected examples from the literature. While the article covers a wide range of literature, it is by no means comprehensive and does not provide detail instructions on how to obtain structures from NMR parameters, such knowledge will require an

Received 4 March 2013; revised 29 January 2014; accepted 29 January 2014

Correspondence to: Julio C. Facelli; E-mail: julio.facelli@utah.edu

Concepts in Magnetic Resonance Part A, Vol. 42A(6) 261–289 (2013)

Published online in Wiley Online Library (wileyonlinelibrary.com). DOI: 10.1002/cmr.a.21291

extensive volume dedicated exclusively on the topic. This article intends to provide molecular structural researchers, new to the field of NMR, with an overall panorama of the potential of using high resolution NMR for structure elucidation when other more traditional techniques are not feasible and/or to complement them. To this end and to emphasize the didactic value of this work, after each section a brief conclusion has been added to recap the critical concepts.

The methods to extract structural information from NMR spectra can be broadly classified as direct and indirect methods. Direct methods are those in which there is an explicit relationship between NMR parameters and the molecular geometry; indirect ones are those in which the relationship is mediated by the electronic molecular structure. We divide this article accordingly into two main sections that describe the methods available for each category and a final section in which we describe the software available for obtaining structural information from NMR parameters.

DIRECT METHODS

Direct methods are based on the explicit dependence of the direct dipolar coupling on the distances between magnetically active nuclei. Two magnetically active nuclear spins interact via a direct dipolar interaction which is analogous to the classical interaction between two magnetic point dipoles, m_1 and m_2 (*1–3*). The direct-dipolar coupling constant, α, characterize the direct interaction,

$$\alpha = \left(\frac{\mu_0}{4\pi}\right)\left(\frac{\hbar}{2\pi}\right)\gamma_{m_1}\gamma_{m_2}\left(r_{m_1m_2}\right)^{-3} \qquad (1)$$

where μ_0 is the permeability constant, $\hbar$ is the Planck's constant and γ_{m_1}, γ_{m_2} are the magnetogyric ratio of nuclei 1 and 2, respectively. It is important to recall that α depends on the average of the inverse cube separation between the magnetic dipoles, $r_{m_1m_2}$. For an isolated spin pair, the direct dipolar contribution to the spin–spin Hamiltonian is

$$\hbar^{-1}\hat{H} = \alpha I_1 . D(1,2) . I_2 \qquad (2)$$

where $D(1,2)$ is the direct dipolar tensor, which averages to zero for rapidly tumbling molecules because it is traceless, i.e. the sum of its diagonal elements is zero.

There are two principal methods that make use of this property for structure elucidation, those based on the Nuclear Overhauser Effect (NOE) (*4*) contributions to the NMR relaxation and those based on the direct measurement of the dipolar couplings. Because the direct dipolar couplings average to zero for rapidly tumbling molecules, the last ones can be used only in either solids or in solution when using liquid crystals (LCs) or strong magnetic or electric fields to induce preferential orientation of the molecules. NOE based methods are restricted to rapidly tumbling molecules in liquids.

Direct Dipolar Coupling in Solids

Considering again the model of an isolated spin pair of nuclei, "1" and "2," interacting with each other via the dipolar–dipolar interaction, only two, of the six terms known as the dipolar alphabet (*5*) are required to predict the NMR spectrum of an isolated spin pair,

$$\hbar^{-1}\hat{H}_{DD} = \alpha\left\{\left[-I_{1z}I_{2z}\left(3\cos^2\theta - 1\right)\right] + \frac{1}{4}\left[I_1^+I_2^- + I_1^-I_2^+\right]\left(3\cos\theta^2 - 1\right)\right\} . \qquad (3)$$

For heteronuclear spins only, the first term in Eq. [3] commutes with the Zeeman Hamiltonian, and it is the only necessary term to predict the NMR spectrum. For a homonuclear spin pair, the second term also commutes with the Zeeman Hamiltonian and must be added to predict the NMR spectrum (*6*). For a stationary sample containing one spin heteronuclear pair, the dipolar interaction produces a power pattern with two horns separated by the dipolar constant, α (see Fig. 1).

The separation between the horns in Fig. 1 contains also a contribution from the anisotropy of the indirect coupling tensor between the spins, but because its magnitude is much smaller, generally can be ignored for atoms of the first and second row. There are several experimental techniques that can be employed for measuring dipolar coupling constants, which subsequently can be used to provide internuclear distances.

Static and Magic Angle Spinning Techniques

The measurement of the direct dipolar couplings in static solids is very limited because for abundant spins,

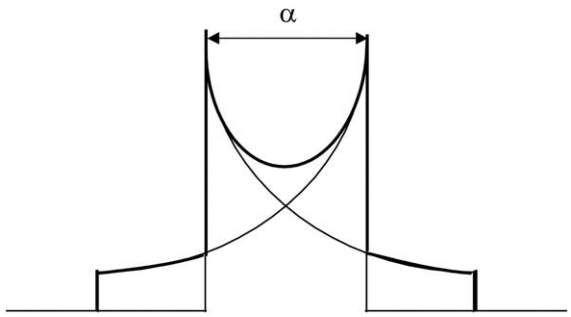

Figure 1 Schematic powder line shape for a one spin in a pair of heteronuclear spins. The splitting between the horns is the dipolar constant, α.

like ^{1}H, the solid-state spectra is very broad and only the momentum of the spectra is available for analysis. This type of spectrum can only be used for crude estimations of average distances (*7*). On the other hand, the spectra of less abundant nuclei, like ^{13}C, typically do not show any evidence of dipolar interactions because the probability of having two magnetically active nuclei in close proximity is very low. In these cases it is possible to use specifically labeled compounds to extract distance information between the specifically labeled nuclei; however, specific labeling is a cumbersome and costly process that is rarely used (*8*).

Biosynthetically site-directed ^{13}C-enriched samples provide an alternative way to measure dipolar couplings in solids. One of the examples of using this approach comes from the early 1980s, when ^{13}C CP magic angle spinning (MAS) NMR spectra contributed much to the understanding of the complex solid-state structure of cellulose. Browna et al. (*9*) investigated a cellulose sample extracted from a sample of wood that was grown in 20% $^{13}CO_2$ atmosphere, such that the carbons sites were partially ^{13}C labeled. They recorded a ^{13}C CP MAS spectrum of the cellulose sample and observed fine structure within each resonance, indicating the presence of amorphous and crystalline regions within the sample.

Several techniques which employ MAS have been developed to recover the dipolar interaction (*10,11*). MAS (*12,13*) is usually employed in SSNMR to remove chemical shift anisotropy (CSA) and as a tool for removing heteronuclear dipolar coupling effects. MAS involves the rapid rotation of the sample about an axis set at angle $\theta_R \approx 54.74°$, where $(3\cos^2\theta_R - 1) = 0$, which averages to zero any anisotropic interaction, eliminating the CSA and heteronuclear coupling from the spectra. However, as these interactions have valuable information about the molecular structure it is desirable to re-introduce or recouple them into the spectra. Jaroniec (*14*) has provided a comprehensive chapter on heteronuclear dipolar recoupling techniques. Among those techniques, rotational echo double resonance (REDOR) (*15,16*), rotational resonance (R^2) (*17,18*), and dipolar recoupling with a windowless sequence (DRAWS) (*19*) permit the measurements of dipolar couplings as small as ≈20–30 Hz. In the following subsections, we briefly explain some of these methods commonly used to recover or reintroduce the heteronuclear dipole interactions under MAS in isolated spin pairs (*14*).

Rotary Resonance Recoupling (R^3) combines the MAS rotation of the sample with the irradiation of the heteronuclear spin system at the Larmor frequency of one of the spin species. The experiment uses the continuous-wave RF irradiation of spin species I_2, for the observation of the NMR signal of I_1. The RF nutation frequency is set to a small multiple of the MAS ω_r frequency ($\omega_2^{RF} = n\omega_r$) (*20,21*). Because of the combined effects of MAS and RF pulse sequences on nuclear spin dynamics, the lowest-order average dipolar Hamiltonian is given by:

$$<\hat{H}_D^{(0)}> = \left(\omega_{D_{12}}^{(-n)} + \omega_{D_{12}}^{(n)}\right)\hat{I}_{1z}\hat{I}_{2z} - i\left(\omega_{D_{12}}^{(-n)} + \omega_{D_{12}}^{(n)}\right)\hat{I}_{1z}\hat{I}_{2y}. \quad (4)$$

The analysis of Eq. [4] shows that for $n = 1$ and $n = 2$, the dipolar coefficients are reintroduced under MAS for RF nutation frequencies, ω_r and $2\omega_r$, which otherwise results in an average $<H_D^{(0)}> = 0$. This method gave place to the development of several related schemes (*14,22,23*), all of them capable to measure heteronuclear dipolar couplings in solids.

Heteronuclear dipolar recoupling can also be achieved by applying sequences of discrete, rotor-synchronized 180° pulse to one or both spin species, which is the basis of the REDOR technique introduced by Guillion and Schaefer (*16*). Under MAS and I_1–I_2 dipolar coupling conditions any I_1 spin transverse magnetization dephases during the first half of the rotor period and then it is refocused during the second half. If 180° pulses are applied during the rotor period to the I_1 spin, the I_1–I_2 dipolar coupling is refocused at the end of every rotor period. In a second experiment, this refocusing of the dipolar coupling is prevented by a series of rotor synchronized 180° pulses applied to I_2 and the I_1 spin spectra is recorded for several different lengths of dephasing time, that are a multiple of $2\tau_R$, where τ_R is the rotor period. The difference between the I_1 spin intensity at the end of the first experiment, i.e. when the magnetization is refocused, and its intensity in any of the second experiments when the magnetization is not refocused depends quantitatively on the dipolar coupling strength and using the explicit formulae given in Refs. *14* and *24* it is possible to estimate the value of the I_1–I_2 dipolar coupling.

Other dipolar recoupling pulse sequence reported in the literature is DRAMA, Dipolar Recovery at the Magic Angle, by Tycko and Dabbagh (*25*), which is used here to show how dipolar recoupling techniques can be developed using the Average Hamiltonian Theory (AHT) (*26*).

AHT is useful to understand the evolution of the magnetization when a sequence of RF pulses is repeated many times, such as in the case of dipolar recoupling experiments. The conditions for applicability of AHT are

$$H_{RF}(\tau_C + t) = H_{RF}(\tau_C) \quad (5)$$

$$H_{\mathrm{D}}(\tau_{\mathrm{C}}+t)=H_{\mathrm{D}}(\tau_{\mathrm{C}}) \tag{6}$$

$$H_{\mathrm{CSA}}(\tau_{\mathrm{C}}+t)=H_{\mathrm{CSA}}(\tau_{\mathrm{C}}) \tag{7}$$

where RF = radio frequency, D = dipolar coupling, CSA = chemical shift anisotropy, and $\tau_{\mathrm{C}}=N\tau_{\mathrm{R}}$ is the cycle time, which should be a multiple of τ_{R} in the recoupling sequences. Under this conditions the evolution operator, is given by

$$U(t)=U_{\mathrm{RF}}(t)\tilde{U}\ (t) \tag{8}$$

with, $U_{\mathrm{RF}}(\tau_{\mathrm{C}})=1$ and using that $|H_{\mathrm{D}}|\tau_{\mathrm{C}} \ll 1$; $|H_{\mathrm{CSA}}|\tau_{\mathrm{C}} \ll 1$; $|H_{\mathrm{iso}}|\tau_{\mathrm{C}} \ll 1$, the new Hamiltonian corresponding to $\tilde{U}(t)$ is easily calculated using the relations

$$i\frac{\partial U(t)}{\partial t}=H(t)U(t) \tag{9}$$

$$i\frac{\partial[U(t)]^{-1}}{\partial x}=-U(t)^{-1}H(t) \tag{10}$$

the spin Hamiltonian results

$$\tilde{H}(t)=\tilde{H}_{\mathrm{D}}(t)+\tilde{H}_{\mathrm{CSA}}(t)+\tilde{H}_{\mathrm{iso}} \tag{11}$$

with

$$\tilde{H}_{\mathrm{D}}(t)=U_{\mathrm{RF}}\ (t)^{-1}H_{\mathrm{D}}(t)U_{\mathrm{RF}}(t) \tag{12}$$

$$\tilde{H}_{\mathrm{CSA}}(t)=U_{\mathrm{RF}}\ (t)^{-1}H_{\mathrm{CSA}}(t)U_{\mathrm{RF}}(t) \tag{13}$$

$$\tilde{H}_{\mathrm{iso}}=U_{\mathrm{RF}}\ (t)^{-1}H_{\mathrm{iso}}U_{\mathrm{RF}}(t) \tag{14}$$

$U_{\mathrm{RF}}(t)^{-1}$ acts on the spin operators of D, CSA, and iso terms, Eqs. [11]–[13], making these spin operator parts time-independent and $U(\tau_{\mathrm{C}})$ can be approximated by

$$U(\tau_{\mathrm{C}}) \approx \exp\left\{-i\int_0^{\tau_{\mathrm{c}}} dt\tilde{H}\ (t)\right\}=e^{-i\tilde{H}_{\mathrm{avg}}\tau_{\mathrm{C}}} \tag{15}$$

As long as the measurements are performed only on the state of the spin system at multiples of τ_{C} (not in the middle of an RF block), it is sufficient to calculate the average Hamiltonian in the interaction representation to determine the NMR signals. There are many sequences of RF pulses that can be used to perform the homonuclear recoupling. Following Tycko (*27*) analysis, it becomes apparent that the time dependence of the spin operators induced by the RF pulses interferes with the spatial time dependence arising from the MAS, which is also periodic in τ_{C}; therefore the NMR signals are determined by $\tilde{H}_{\mathrm{avg}}$ alone. Pulse sequences for which the time-averaged dipole–dipole coupling is non-zero, but the time averages for other interactions (chemical shifts, heteronuclear couplings, etc.) are zero, can be used to measure homonuclear couplings using recoupling techniques.

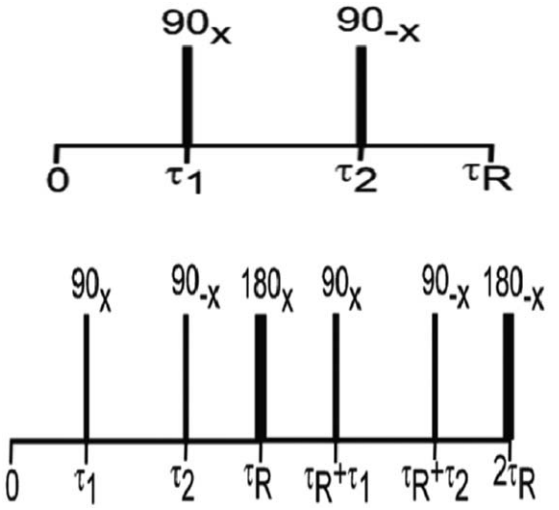

Figure 2 Upper: Simple DRAMA pulse sequence; Bottom: longer DRAMA pulse sequence with additional 180° pulses.

The DRAMA (*25*), Fig. 2, consists of two 90° pulses symmetrically placed in each rotor period and works in the delta-function pulse limit, i.e. when the RF pulse lengths are negligible compared with τ_{R}.

This sequence produces a recoupling of the dipolar interaction as well as the CSA and average chemical shift. The addition of 180° pulses that do not affect the dipolar interaction produces therefore the desired effect. For the pulse sequence (Fig. 2 bottom) over a period $2\tau_{\mathrm{R}}$, $\tilde{H}_{\mathrm{CSA}}(t)$ and $\tilde{H}_{\mathrm{iso}}$, averages to zero because the 180° pulses change signs of $\tilde{H}_{\mathrm{CSA}}$ and $\tilde{H}_{\mathrm{iso}}$ in the second rotor period. $\tilde{H}_{\mathrm{D}}(t)$ is not affected by the additional 180° pulses and the average dipole–dipole coupling is

$$\begin{aligned}\tilde{H}_{\mathrm{D\,avg}}=3\left(I_{y1}I_{y2}-I_{z1}I_{z2}\right)\Bigg\{&\frac{A}{2\pi}[\sin(\omega_{\mathrm{R}}\tau_2+\gamma)\\&-\sin(\omega_{\mathrm{R}}\tau_1+\gamma)]\\&-\frac{B}{2\pi}[\cos(\omega_{\mathrm{R}}\tau_2\gamma)-\cos(\omega_{\mathrm{R}}\tau_1+\gamma)]\Bigg\}\\&+\frac{C}{4\pi}[\sin(2\omega_{\mathrm{R}}\tau_2+2\gamma)-\sin(2\omega_{\mathrm{R}}\tau_1+2\gamma)]\\&-\frac{D}{4\pi}[\cos(2\omega_{\mathrm{R}}\tau_2+2\gamma)-\cos(2\omega_{\mathrm{R}}\tau_1+2\gamma)]\end{aligned} \tag{16}$$

which explicitly shows how the dipole–dipole couplings are now selectively recoupled.

Other possible pulse sequence, Fig. 3, named 2Q-HORROR (*28*) (double quantum homo nuclear rotary resonance), consists of a block of continuous RF irradiation at $\omega_1 = \omega_{\mathrm{R}}/2$ for an even number of rotor periods. The cycle is a $90_y-360_x-90_{-y}$ sequence, with delta-function 90° pulses, and a very long, weak 360° pulse.

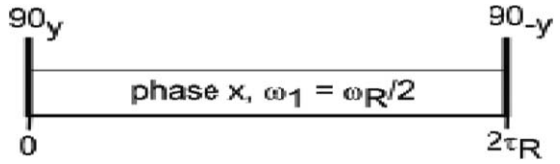

Figure 3 Pulse sequence for 2Q-HORROR recoupling.

This sequences averages isotropic and anisotropic shielding to zero, and in this case the dipolar average Hamiltonian is,

$$\tilde{H}_{\mathrm{D\,avg}} = \frac{3}{8}[(I_{+1}I_{+2}+I_{-1}I_{-2})(A\ \cos\gamma + B\sin\gamma) + i(I_{+1}I_{+2}-I_{-1}I_{-2})(-A\ \sin\gamma B\cos\gamma)] \quad (17)$$

which shows that 2Q-HORROR produces pure double-quantum recoupling, with recoupled interaction proportional to $(A^2+B^2)^{1/2}$, and hence independent of γ. Recoupling sequences with this property are called γ-encoded. The pulse sequence SEDRA (*29*) (simple excitation for the dephasing of rotational echo amplitudes) or RFDR (*30,31*) (RF-driven recoupling), is depicted in Fig. 4.

In this sequence when the isotropic and the anisotropic chemical shifts differences are small, the pulse sequence causes dipolar recoupling with no chemical shift or CSA recoupling, if the pulse lengths are a significant fraction of τ_R. The resulting average dipolar Hamiltonian is

$$\tilde{H}_{\mathrm{D,avg}} = \left\{ \frac{3(\omega_R^2+4\omega_1^2)}{16\pi(\omega_R^2-4\omega_1^2)}[\sin(\omega_R\tau_P+\gamma)-\sin\gamma]A - \frac{3(\omega_R^2+4\omega_1^2)}{16\pi(\omega_R^2-4\omega_1^2)}[\cos(\omega_R\tau_P+\gamma)-\cos\gamma]B + \frac{3(\omega_R^2+\omega_1^2)}{16\pi(\omega_R^2-\omega_1^2)}[\sin(2\omega_R\tau_P+2\gamma)-\sin2\gamma]C - \frac{3(\omega_R^2+\omega_1^2)}{16\pi(\omega_R^2-\omega_1^2)}[\cos(2\omega_R\tau_P+2\gamma)-\cos2\gamma]D \right\} [3I_{z1}I_{z2}-I_1.I_2] \quad (18)$$

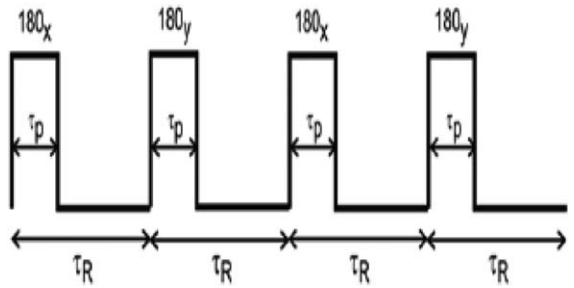

Figure 4 RF pulse sequence for RFDR.

where τ_P is the π pulse length and $\omega_1 = 1/2\ \tau_P$. An useful advantage of RFDR is that $\tilde{H}_{\mathrm{D,avg}}$ is proportional to $[3I_{z1}I_{z2}-I_1.I_2]$, which is the same behavior found for a static sample**.** Because of that, homonuclear dipoledipole techniques can be adapted to MAS experiments including time-reversal multiple-quantum spectroscopy (*32*) and homonuclear decoupling (*33*). RFDR also permits sensitivity-enhanced two-dimensional solid-state NMR with transverse mixing (*34*).

In the previous sections, we have provided references and a brief explanation of a number of useful and widely available techniques to measure the dipolar coupling in either static of MAS solid samples. Each technique has different advantages and disadvantages, therefore researchers should consult the literature to find the best techniques suitable for their problem. Moreover, it is important to remark that the measured dipolar couplings include a small contribution of the anisotropic part of the indirect couplings, which usually is quite small and can be ignored in the analysis as well as a dynamic averaging component that needs to be taken into account when comparing interatomic distance obtained by other methods.

Nuclear Magnetic Resonance Spectroscopy in Liquid Crystals

A LC is a state of matter that has properties between those of a conventional liquid and crystalline solid. The LC may flow like a liquid, but its molecules may be oriented in a crystal-like way (*35*). Different types of LC phases can be distinguished by their different optical properties such as birefringence. When viewed under a microscope using a polarized light source, different LC phases will appear to have distinct textures. The contrasting areas in the textures correspond to domains where the LC molecules are oriented in different directions, but within a domain the molecules are well ordered.

NMR is one of the experimental techniques used since the 1960s to study these systems and/or molecules dissolved in them. Reference *36* contains the latest state-of-the-art developments in using NMR for LCs.

The most common use of LC for structural determination is its use as a solvent that can induce preferential order in small molecules dissolved in it. The partial ordering induced in the solute leads to reduced, but measurable, dipolar couplings, among the protons of the dissolved molecule. Using these dipolar couplings, it is straightforward to get structural information using the explicit dependence of the dipolar couplings (Eq. [1]) on interatomic distances between the interacting nuclei. In order to accurately obtain the necessary

dipolar couplings, the critical step is to assign the experimental spectra, which can be extremely complicated for systems of large number of non-equivalent spins.

One of the methods used to address the assignment problem is multiple-quantum NMR (MQ-NMR). A typical example of its use in LC NMR spectroscopy has been provided recently by Burnell et al. (*37*). His work demonstrates the use of LC NMR to solve the structures of solutes with more than eight spins using MQ-NMR to simplify the spectra. The idea of MQ-NMR is to use transitions that involve the mutual flip of many spins. When the number of spins flipped approaches the number of spins in the molecule, the number of possible transitions is greatly reduced (*38*). Burnell et al. (*37*) exemplified the idea for the case of benzene, see Fig. 5.

The normal 1Q spectrum consists of 74 lines, with no regular patterns, while the 6Q spectrum is a single line, involving the flip of the six spins; the 5Q spectrum is a doublet because the simultaneous flip of five spins occurs in two equivalent transitions: $|\alpha\alpha\alpha\alpha\alpha\alpha\alpha> \rightarrow |\alpha\beta\beta\beta\beta\beta\beta>, |\alpha\alpha\alpha\alpha\alpha\alpha\alpha> \rightarrow |\alpha\beta\beta\beta\beta\beta\beta>$ and $|\alpha\alpha\alpha\alpha\alpha\beta> \rightarrow |\beta\beta\beta\beta\beta\beta\beta>, |\alpha\alpha\alpha\alpha\alpha\alpha\alpha> \rightarrow |\alpha\beta\beta\beta\beta\beta\beta>$, and $|\alpha\alpha\alpha\alpha\alpha\alpha\beta> \rightarrow |\beta\beta\beta\beta\beta>$. The 4Q spectrum is built by three triplets indicating the three ways of choosing two spins that are not flipped, that is, those that are *meta*, *ortho*, or *para* respect to each other. The central line of this triplet involves the 4Q coherences between spin states such as $|\beta\alpha\alpha\alpha\alpha\alpha\alpha>$ and $|\alpha\beta\beta\beta\beta\beta\beta>$. Using the information from the simplified spectra of the three highest order MQ it is possible to completely assign the low order MQ spectra and obtain the dipolar couplings that dominate it.

In the MQ experiment, a first pulse generates observable magnetizations X and Y from the equilibrium Z magnetization and other unobservable 1Q coherences. After a waiting time, those magnetizations evolve and the application of a second radiation pulse converts all these coherences into all MQ coherences of all orders. The MQ coherences evolve between the second pulse and the application of a third pulse, that rotates some of the MQ coherences back to unobservable 1Q coherences, which, after further evolution form an observable echo at a time τ after the third pulse. By application of Fourier transform to the echo amplitude as a function of t_1, the time between the second and third pulses, the spectrum containing all MQ orders as shown in Fig. 5 is generated. In practice, a two dimensional experiment is performed in which an echo signal is collected for each increment of t_1, and the absolute value of the double Fourier transform with respect to t_1 and t_2 is projected onto the F_1 axis to give the MQ spectrum. Several schemes, not described here, have been employed to improve the digital resolution by the selective detection of one order at a time (*38–40*).

In Ref. *37*, the authors show several examples for which the MQ-NMR spectra proved to be a valuable tool to interpret the 1Q spectrum and obtain the corresponding dipolar couplings. These examples are: (i) 2,6 dichloro-1-ethenylbenzene, Fig. 6, for which the

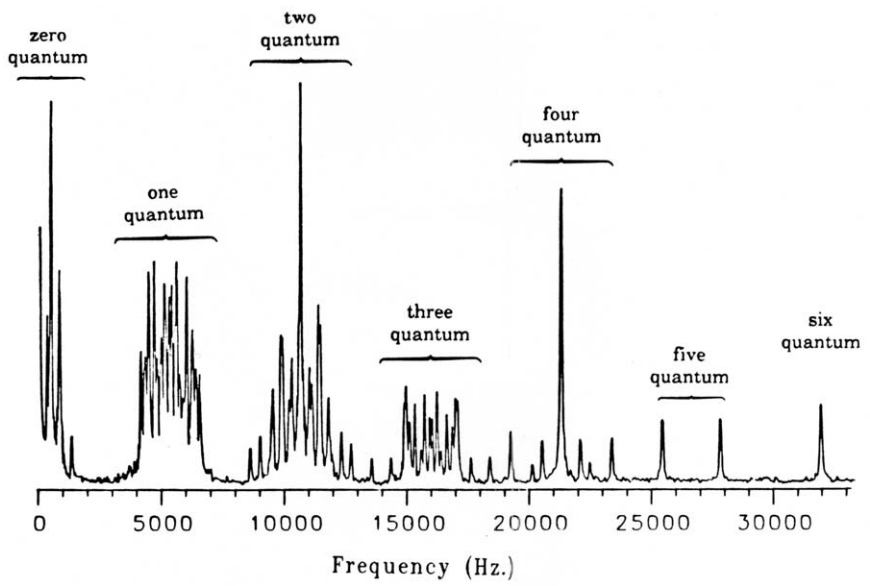

Figure 5 The multiple-quantum spectrum of benzene dissolved in *N*-(4-ethoxy-benzylidene)-4′-*n*-butylaniline (EBBA) obtained using pulse sequence. Reproduced from Ref. *37*, with permission from World Scientific Publishing.

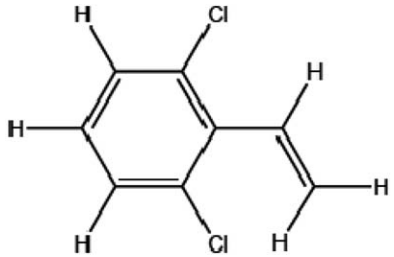

Figure 6 Schema of 1,3-dochloro-2-ethenylbenzene.

unknown dihedral angle between the ethenyl group and the benzene ring leaving a spectrum with five unknown order parameters. It is easy to assign the wings of the spectrum (see Fig. 7) to the aromatic protons, but the problems arise in the central clump of transitions (group c in the figure). This central part of the spectrum, corresponding to the ethenyl protons, could be assigned once the MQ spectrum was obtained and solved (*41,42*). In this example, the outer lines of the 1Q NMR spectrum involve only aromatic protons, then it is possible to excite MQ-coherences among the three aromatic protons (frequency selective for the outer parts of the spectrum). The highest order spectrum observed is the 3Q spectrum that consists of eight transitions which depend on the long-range dipolar couplings between aromatic and ethenyl protons. (ii) Another example presented in the literature is biphenyl

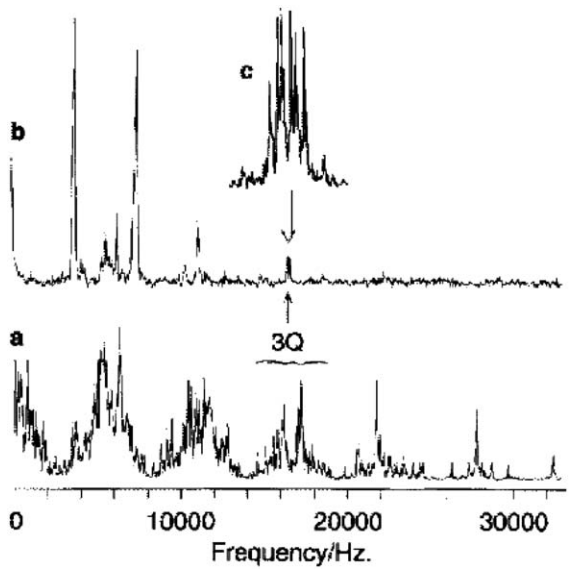

Figure 7 (a) The 400 MHz non-selective MQ-NMR spectrum of 1,3-dochloro-2-ethenylbenzene. (b) The 400 MHz selective MQ-NMR spectrum of 1,3-dochloro-2-ethenylbenzene. (c) Expanded view of the 3Q region noted in (b). Reproduced from Ref. *41*, with permission from Academic Press.

(*41,42*), which is interesting because it is present in almost all LCs. There are 10 spins and the 1Q spectrum is very complicated because the dihedral angle may be affected by the anisotropic environment. In this case, the 8Q-NMR spectra was used to provide starting parameters to resolve the 1Q high resolution spectrum (*43*); finally (iii) butane is the most difficult solute for which the 1Q spectrum has been analyzed by MQ-spectrum techniques. The difficulties arise from the presence of 10 spins, three conformers (two of them related by symmetry) and three unknown order parameters for the two independent conformers. In addition, the population of the conformers is unknown and depends on the interaction between the solute and the surrounding molecules. The 7Q and 8Q spectra were used to assign almost all the transitions in the 1Q highly NMR spectrum of this compound leading to a fully resolved structure of butane dissolved in a LC (*40*).

The other approach to obtain dipolar couplings from complex spectra dominated by the dipolar couplings from small molecules dissolved in LC is the use of automated computer routines to efficiently search the parameter space in order to find unique values of spectral parameters that fit the experimental high resolution NMR spectrum. Some of the automatic tools available for the analysis of NMR spectra of oriented molecules are the DANSOM code (*44*) and the software implemented by Cosenza's group (*45*), which have achieved some success, but still always need significant operator intervention to avoid trapping in a local minima. In recent years, there have been new advances by implementing sophisticated and robust Genetic Algorithm (GA) procedures (*46*) to fit highly anisotropic NMR spectra, avoiding the problems encountered with previous automated procedures. The GA methods circumvent the problem of trapping in local minima requiring minimal operator intervention. For instance, Burnell et al. (*37*) employed a two-step GA procedure for solutes belonging to various categories of increasing complexity, including (i) rigid solutes with a single conformation, e.g. eight spin system like azulene and biphenylene, (ii) solute molecules interconverting between symmetry related conformers, e.g. *p*-bromobiphenyl, and (iii) solute molecules interconverting between non-symmetry related conformers, e.g. the ten spin system butane (*47*). The two-step procedure consists in a first GA-fitting of the chemical shifts and order parameters until some resemblance between experimental and calculated spectra was obtained. From this assignment, dipolar couplings were estimated and used as the starting parameter set for a second GA-fitting. A weakness of this procedure is that it attempts a global optimization without any strategy, which is a serious difficulty when the parameter's search space is

very extensive. To address this problem Burnell et al. (*37*) also have implemented an Evolutionary Algorithms (EAs) technique (*48*), which is more robust than the GAs and converge faster. For the case of *n*-pentane, Burnell et al. (*37*) employed the Covariance Matrix Adaptation Evolution Strategy (CMA-ES) (*49*), which in spite of the large density of lines that prevented from removing the background was very successful in obtaining a perfect fit of the observed spectrum.

In conclusion, with the development of modern MQ experimental methods and automatic spectral analysis techniques based on evolution strategies the NMR LC method can be extended to large and complicated solutes. Still the use of LC for measuring dipolar constants is seriously curtailed by poor solubility of many compounds in commonly available LC. Once that the dipolar couplings are obtained using LC techniques, the estimation of the interatomic distance faces the same problems discussed above, vibrational averaging and discrimination of the contribution from the anisotropic part of the indirect couplings.

Structure Refinement with NOEs

NOE manifests in the change of the intensity of the resonance lines by dipolar cross-relaxation from neighboring spins with perturbed energy populations. For instance, when a proton or any other nuclei (A) with spin greater than zero is close to another proton (X), their magnetic dipoles interact directly and the dipole–dipole interaction, DD, produces cross-relaxation. Because the dipolar interaction is inversely proportional to the cube of the effective inter-spin distance, the NOE is dependent on the distance between the nuclei. NOE (*4*) is the transfer of nuclear spin polarization from one nuclear spin population to another via the cross-relaxation mechanisms produced by the DD interaction. The NOE effect depends on the presence of a secondary irradiation radio-frequency (*B*1), which causes the alteration of the normal spin population and intensities of the observed (not irradiated) nuclei (A).

To understand the nature of the NOE effect, consider the system of two spins in Fig. 8; for simplicity the spins are not coupled. The system has four energy spin states αα, αβ, βα, ββ, labeled according to the spin states of the two spins. The DD allows transitions with probabilities: ω_1, for a single spin flip of only one of the two spins (A or X); ω_0 involving simultaneous spin flip α→β for one spin and β→α, for the other one (zero quantum transitions); and ω_2 involving spin flip of both spins in the same direction, corresponding to a net double-quantum transition. When the X transition is irradiated, the populations of the αα and αβ states and the βα and ββ states become, respectively, identical. This corresponds to the saturation situation of the spin populations. During the corresponding relaxation process, the difference between those two populations depends on which relaxation mechanism dominates. If $\omega_2 > \omega_1$, ω_0, then the βα/ββ population will tend to that of the ββ state, and the αβ/αα will tend to that of the αα state. Then, if the equilibrium value for the A population difference is Δ, the new population difference for the A transition is 2Δ. This process is named positive NOE. If ω_0 dominates, βα/ββ population will tend to that of the βα state, and αβ/αα will tend to that of the αβ state, i.e. population difference tends to zero and there is no NOE.

If ω_1 is the only relaxation pathway, the irradiation of X will induce transitions until its population is equalized without affecting A. However, the other two

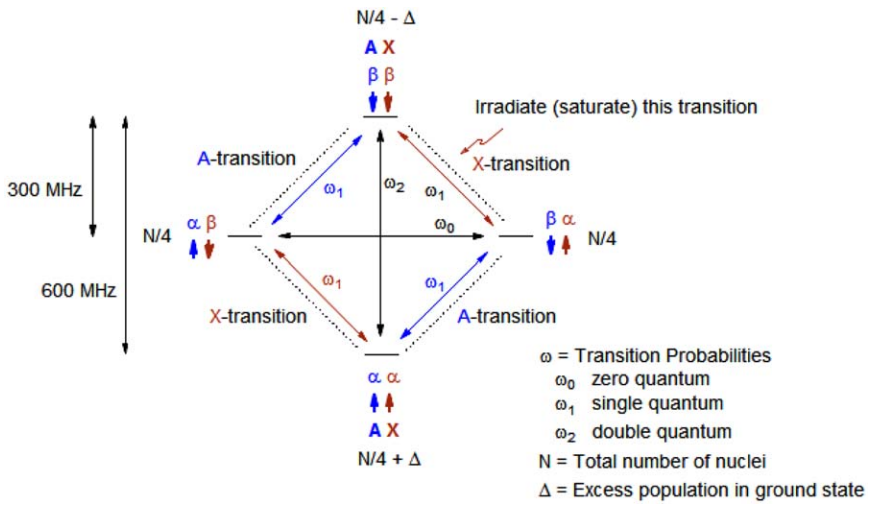

Figure 8 Schema of NOE transitions from (http://www.chem.wisc.edu/areas/reich/nmr/08-tech-02-noe.htm), © Copyright Hans J. Reich 2011, University of Wisconsin.

mechanisms will affect A, with X polarization going back from saturation to the Boltzmann equilibrium; the ω_0 mechanism will cause the neighboring (so far unperturbed) spin to deviate from its Boltzmann equilibrium toward a decrease in the α, β population difference. This process will result in a decrease in the A signal intensity, that is a negative NOE.

Because the direct dipolar interaction drops off very fast with the distance between interacting nuclei, the ^{1}H NOE is detectable only for protons at a distance shorter than 5 or 6 Å. If we consider a 500 MHz spectrometer, the corresponding ω_1 mechanism requires frequencies of 500 MHz to induce transitions, the ω_2 mechanism (corresponding to the simultaneous flip of two ^{1}H spins) requires fields of 1,000 MHz, and ω_0 frequencies are very close or equal to the resonance frequency difference between the two protons, only a few ppm (100–1000 Hz).

The first NOE experiment consisted on the decoupling of one proton for a few seconds and then measuring a spectrum (*4*). The following step was a careful peak integration to show which proton resonances were enhanced and, in consequence, close to the decoupled one. Unfortunately, when employing this technique only very large NOE effects could be reliably detected and its most common use has been for the determination of stereochemical and conformational relationships on relatively rigid molecules.

The current methodology for obtaining NOE spectra involves different schemes based on pulse gradient methods in which enhanced signals are clearly detected. Description of NOE experiments for both conformational and population analysis can be found in Ref. *50*. Gradient NOE experiments do not give as large a NOE enhancement as steady-state experiments, but their advantage over steady-state experiments arises from the fact that gradient NOE experiments are not difference experiments. The absence of subtraction artifacts means that much smaller NOEs can be reliably measured in gradient experiments.

The cross-relaxation rate between the A and X spins is the phenomena by which the magnetization of two different spins are connected. The cross relaxation rate constant is σ_{AX}, $\sigma_{AX} = \omega_2 - \omega_0$. It depends on the type of the nuclei involved, on their distance, r_{AX}, on the NMR field, and on the characteristic time, named the correlation time for reorientation of the vector AX. The normalized NOE intensity between the spins is proportional to the cross-relaxation rate between A and X spins, which is proportional to r_{Ax}^{-6}.

$$\sigma_{Ax} = k r_{Ax}^{-6} \tag{19}$$

Considering that the factors defining k depend on the correlation time, the Larmor frequency, and the magnetogyric ratio, which remain constant in a given selective inversion experiment, the relation between the intensities of a pair of NOE signals can thus be assumed proportional to the ratio of their inter-nuclear distances:

$$\frac{I_{1x}}{I_{2x}} = \frac{r_{A1x}^{-6}}{r_{A2x}^{-6}} \tag{20}$$

Then it is only necessary to know one inter-nuclear distance, r_{A1X}, in order to determine a second one. This is the basis on which all distance measurements are made using the NOE.

The experimental techniques for measurement of NOEs have developed a great deal with new experimental methods, like transient DPFGSE NOE, zero-quantum filtration, and hardware improvements, like non-quadrature detection, improved RF generation, digital receivers, etc., becoming widely available (*51*). The progress in the experimental methods and hardware improvements is such that the lack of accuracy in NOE distance measurement arises from other factors affecting the NOE intensities, like additional cross-relaxation pathways or spin diffusion, selective polarization transfer from inhomogeneous inversion, and variations in the effective correlation time.

The usual recipe for adding NOEs information to solve molecular structures consists of: (i) acquiring a NOE spectra and picking peaks to get a list of NOE cross peaks, removing artifacts and noise and (ii) assigning the NOE peaks selected as restraints for structure minimization (*52*). These steps are usually performed iteratively, where the first peak list contains a large number of ambiguous peaks that are not taken into account and very crude structures that are evaluated using only unambiguous peaks. These crude structures are used to filter ambiguous peaks and to discard those structures that are clearly not consistent with any physically plausible structure. This procedure is repeated making reassignments of restraints as necessary. The restraint set is therefore refined in each iteration step; the process continues until the structure is validated. The process to automate NOE interpretation is very important. Automated methods help to avoid mistakes in data interpretation in benefit of a correct structure determination and speed up of the process of structure determination. These methods have become indispensable for large structures, for which the great number of NOEs cannot be processed manually (*53*,*54*).

The process described above is routinely applied to solve bio-molecular structures in the range of 40–100 kDa via NMR. For instance in the Protein Data Bank (PDB; http://www.rcsb.org/pdb/), which is the single

largest worldwide archive of structural data of biological macromolecules, NOE experimental data have been employed to elucidate 25% (in 1994) to 70–80% (now days) of the structures available. These structures include nucleic acids, protein/ligand complexes, proteins that bind two ligands simultaneously, giving structural information on their relative orientation, proteins with both ligands bound at the same site, and ligands bound to systems as large as ribosomes, tRNA, etc. (*55–57*).

In this section, we have presented the principles of NOE and pointed the reader toward a few applications of using NOEs for structural elucidation. As indicated above NOEs are widely used for structure determination, mostly for bio-organic compounds of medium to large sizes. NOE studies are limited by the usual problems encountered in many NMR techniques, low sensitivity, poor resolution, and lack of adequate solubility of compounds under study. Nonetheless, NOE structure determination is the preferred method for determining the structures of large bio-organic molecules when single crystal samples of the molecule cannot be obtained.

INDIRECT METHODS

All the indirect methods are based on the intrinsic dependence, mediated through the electronic structure, of J couplings and shielding constants on the atomic coordinates of the atoms in a molecule or crystal with magnetically active nuclei. The chemical shift is the change observed in the Larmor resonance frequency on nuclei within a molecule with respect to the bare nucleus resonance frequency. This change is due to the induction of electronic currents by the external and nuclear spin magnetic fields (*58*). The J or indirect dipolar couplings are the result of the interaction between the magnetic moments of equivalent nuclei in a molecule. This interaction is mediated by the mutual polarization of the electron cloud due to its polarization by the magnetic moments of the nuclei, thus the name indirect (*59*).

Because both the chemical shifts and the J coupling are intrinsically quantum mechanical properties, to uncover their relationships to the molecular structure requires complex quantum mechanical calculations that can relate NMR spectral properties with molecular and crystal structure. In this article, we refer alternatively to calculated shieldings and/or measured chemical shifts, the relationship between these quantities have been discussed extensively in other reviews that interested readers should consult (*60*). In the following sections, we discuss how the measurement and calculation of J couplings and chemical shifts can be used synergistically to gain insight on different molecular structural features: chemical bonding, stereo configurations, bond lengths, bond angles, dihedral angles, and packing and symmetry.

Chemical Bonding

Both shielding constants and J couplings are highly dependent on chemical bonding. Here we provide examples of how NMR shieldings and J couplings have been used to determine the bonding of certain magnetically active nuclei in different phases.

One of the earliest solid-state MAS spectra showed that PCl_5 in its stable form actually exists as a mixture of PCl_4^+ and PCl_6^-, contrary to what has been observed in earlier solution-state NMR but consistent with the crystal structure (*61,62*). The solution-state ^{31}P-NMR showed one resonance at 80 ppm, whereas in the solid state there were two resonances observed at -96 and 281 ppm. A similar situation was observed in the coordination of a phospha-alkene ligand to platinum: in solution state a η^2-complex was observed whereas by solid-state measurements a η^1-complex was determined to exist, again confirmed by a X-ray structure (*63*). A difference of 278 ppm is observed in the chemical shift of the phospha-alkene phosphorus between the two bonding arrangements, allowing the assignment of the type of bonding and therefore the molecular structure to be readily made. These examples serve as illustrations of the importance of using solid-state NMR measurements to confirm the chemical bonding of a sample in the solid state, instead of assuming that it will be the same as in solution.

While the above examples show drastic changes in bonding arrangements leading to very large changes in chemical shifts between solution and the solid state, often more modest changes are observed. One of such cases is the chemical shift of the carbonyl carbon in carboxylic acids, which has been shown to depend on the protonation state of this group (*64*). This effect, observed in a series of amino acids and di-peptides in both the protonated and deprotonated forms, has been measured as a small change of around 4 ppm in the measured isotropic shift. The δ_{11} and δ_{22} components of the shielding, however, show much larger changes, with the former changing from 242 to 257 ppm and the latter from 177 to 155 ppm on average in a set of approximately 35 amino acids and amino acid•HCl compounds. These large, reproducible changes allow for a reliable method to assign a protonation state of a carboxylate carbon on the basis of the NMR measurement of the ^{13}C chemical shift principal values.

The chemical shift measured or calculated for compounds with multiple tautomeric forms can provide valuable information on the form that exists or on any

tautomeric averaging that might be occurring. As with the case of conformational averaging that will be discussed below, there are many cases where averaging occurs in solution but in the solid state only one form exists, especially if the spectrum is recorded at low temperatures. As shown in Fig. 9, a series of ^{15}N shielding calculations show distinct changes in both the isotropic and the principal components between a protonated and non-protonated nitrogen in both five-membered and six-membered nitrogen heterocyclic compounds (*65*).

The examples presented here are powerful examples on how sensitive the chemical shifts are to the chemical bonding of the observed nuclei. While the examples show the interdependence of chemical shift and bonding and how using quantum mechanical calculations it

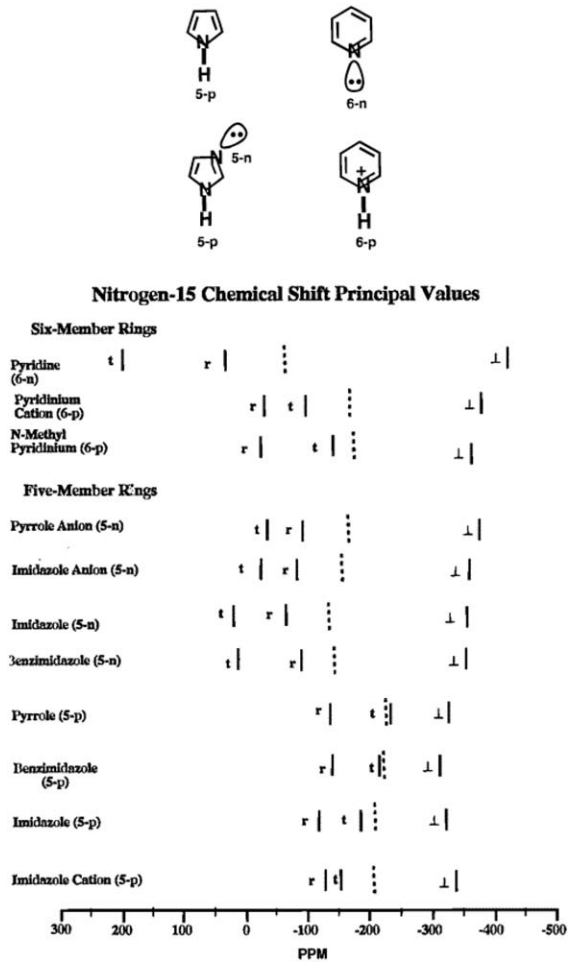

Figure 9 Schematic of nitrogen types in five-member and six-member heterocyclic rings along with typical isotropic (dotted lines) and principal components (solid lines) for representative compounds of each type. (Reproduced from Ref. *65*, with permission from American Chemical Society).

is possible to infer changes in the chemical bonding due to either chemical substitution or media effects or phase changes. Unfortunately, there is no "off the shelf" tool to do this analysis, which requires judiciously selecting calculations that may prove or disprove certain hypotheses about the chemical bonding of the nuclei under consideration. The most effective manner to build the possible hypothesis for testing is by comparison of the experimental results with those available in the literature.

Experimental ^1J(CH) and ^1J(CC) couplings have been used as indicators of sp hybridization for a long time. For instance, in a series of hydrocarbons and hetero substituted hydrocarbons ^1Js were related through regression analysis to maximum bond order hybrid orbital (MBOHO) parameters obtained with the complete neglect of differential overlap (CNDO/2) approach (*66*). In hydrocarbons, Muller and Pritchard (*67*) found a linear relationship between ^1J(CH) and the *s* character, $(s\%)_C$ Eq. [21] and Table 1, of the C—H bond at the C atom.

$$^1J(\mathrm{CH})(\mathrm{Hz}) = a(s\%)_C + b \qquad (21)$$

A similar correlation for ^1J(CC) couplings (*68*), when couplings in single and multiple bonds were included in the analysis, leads to a $\sigma = 6.43$ Hz in Eq. [22].

$$^1J(\mathrm{CC})(\mathrm{Hz}) = a(s\%)_{C1}(\%s)_{C2} + b \qquad (22)$$

but when separate regression analyses for single and multiple CC bond (*68*) were considered, σ values of 2.72 Hz and 5.42 Hz were obtained, respectively. Since only ^1J(CC) values in the 30–50 Hz range were included, substituent and structural effects may well be within the σ limit.

Regression coefficients in Eq. [22] adapted to $^1J(C_bSi)$ couplings between a bridgehead C_b nucleus and a Si one in substituted $Si(CH_3)_3$-polycyclic hydrocarbons were also determined, where the *s*% character

Table 1 Selected ^{1}J(CH) Couplings in Heterosubstituted Hydrocarbons as Given by Eq. [21] and Corresponding Experimental Values (in Hz)

	Equation [3]	Exp.
CH_4	130.47	125
$H_3C—CH_3$	127.0	124.9
$H_3C—C\equiv CH_3$	128.72	131.0
$H_3C—NH_2$	135.6; 131.8	133
$H_3C—C\equiv N$	126.42	136
CH_3F	143.72	149
CH_2F_2	160.57	184.5
CHF_3	172.13	239.1

From Ref. *67*.

for the Si—C bond at each atom were calculated at the AM1 level (*69*). When the parent compounds regression analysis for $^1J(C_bH)$ couplings was considered using linear relationships between $(s\%)_{C(b)}$ and net charges on both the Si and C atoms, correlation coefficients of 0.99 and 0.92, respectively, were obtained.

While the examples provided here derive from fairly old work in the field they are a good illustrations on how the measurement of *J* couplings can be related to chemical concepts of great interest to physical organic chemists. These relationships between bond character and *J* couplings have been extended to large number of nuclei and bonding situations, but space limits our ability to report all of them in this article. Structural chemists interested in exploring this relationships should consult for instance the extensive literature from Contreras et al., who have explored how chemical bonding affects the transmission of spin polarization, which lead to J couplings, thought the electron cloud (*70–72*).

In conclusion, this subsection demonstrates how sensitive the chemical shifts and the coupling constants are to the chemical bonding. We presented a few examples on how this dependency can be used to elucidate chemical bonding and while there is no universal strategy, a careful combination of experiments and calculations can provide insights that otherwise cannot be easily obtained by other spectral methods, making NMR a desirable technique to study chemical bonding.

Stereo Configurations

The reliable determination of stereocenters contained within chemical structures usually requires utilization of NMR data, chemical derivation, molecular modeling, quantum-mechanical (QM) calculations and, if available, X-ray analysis. These are laborious and expensive techniques. Elyashber et al. (*73*) demonstrated that the number of stereoisomers that need to be thoroughly investigated can be significantly reduced by the application of NMR chemical shift calculations to the full set of possible stereoisomers. The authors have shown that from all $2^5 = 32$ stereoisomers generated for artarborol using a fragmental approach based on the HOSE codes (*74*), the constrains imposed by the calculated ^{1}H and ^{13}C chemical shifts leave only four (Fig. 10) possible candidates to be analyzed further, with a considerable reduction of the effort needed for the determination of the observed stereoisomers.

This example and others existing in the literature show that while NMR alone cannot completely solve stereo configuration problems, suitable NMR calculations coupled with experimental measurements can greatly reduce the possible number of stereoisomers greatly reducing the additional work needed for a final determination of their stereochemistry.

Bond Lengths

The dependence of the chemical shift on the bond length has been explored with shielding surfaces and/or plots of chemical shift versus bond length for a variety of diatomic and other small molecules (*75,76*). The use of theory is critical in the study of how chemical shifts are influenced by bond length because a series of quantum chemical calculations changing a specific bond length can be readily done, while this task is nearly impossible to do experimentally for a significantly large range of bond lengths without introducing other changes that will also affect the chemical shifts. It should be noted that experimentally the dependence of chemical shifts on bond lengths can be explored, over a narrow range of bond lengths and for small molecules with the use of isotopic labeling (*77,78*). These experiments and calculations can also serve to show the effect of rotational/vibrational stretching of bonds on the chemical shift (*79*).

Results are typically reported as derivatives of the nuclear shielding with respect to bond length, $\partial^n\sigma/\partial r^n$. The first derivative is nearly always found to be negative, i.e., chemical shifts move to higher values as the bond length is increased, and its magnitude depends both on the atoms involved and the type of bonding. It

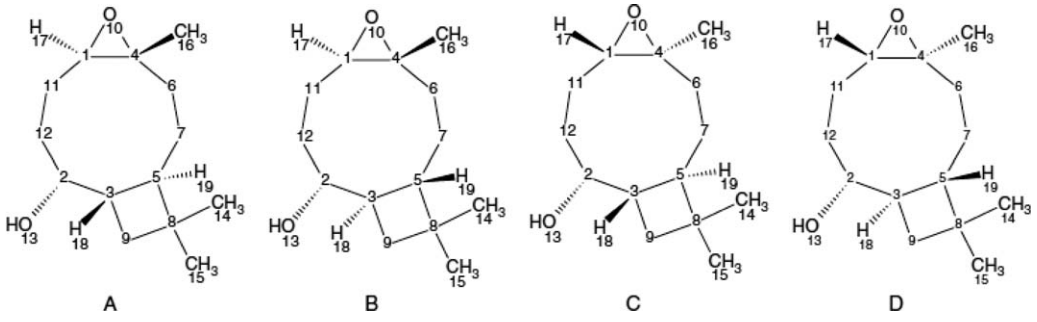

Figure 10 Stereoisomers of artarborol which are consistent with the calculated ^{1}H and ^{13}C chemical shifts. From Ref. *74*

should also be noted that while the dependence of chemical shift on bond length is not linear over a large range, for practical purposes (in the vicinity of typical bond lengths for a given atomic pair and bonding type) it can be treated as such. The general observed trends are: (i) the first derivatives become smaller when one of the atoms is hydrogen versus when both are heavy atoms and (ii) as the multiplicity of the bond increases the magnitude of their derivatives becomes larger (*76*). In the case of carbon isotropic chemical shifts, these derivatives are in the range of about −50 ppm/Å for C—C single bonds and about −300 ppm/Å for multiple or aromatic C—C bonds. This type of analysis has also been expanded to the study of more complex molecules such as amino acid residues, (*80*) where calculations have been done to explore the dependence of the C^{α} and C^{β} chemical shifts on various bond lengths in glycine, alanine, and valine. The magnitude of the calculated derivatives highlights the need to have accurate geometries when using shielding calculations to interpret experimental results.

Grant's group explored the sensitivity of the calculated chemical shift tensor components to C—H bond distances and showed that in a number of different molecules, perylene (*81*), acenaphthene (*82*), pentaerythritol (*83*), and methyl-β-D-glucopyranoside (*82*), the agreement between theoretical shielding values and experiment chemical shifts could be substantially improved by using the most exact information available for the hydrogen atom positions. As is widely known, X-ray diffraction generally does not provide accurate positions for hydrogen atoms, whereas neutron diffraction does; therefore, the best agreement is obtained by using neutron diffraction structures when available. In the absence of neutron diffraction structures, the use of theory to optimize the position of hydrogen atoms in an X-ray structure is shown to be the best option. In most cases, the improvement in the agreement between experiment and theory is substantial; for example, in pentaerythritol (*83*), as shown in Fig. 11, using the X-ray structure for all atom positions gives an rms difference of 4.45 ppm between experimental and theoretical

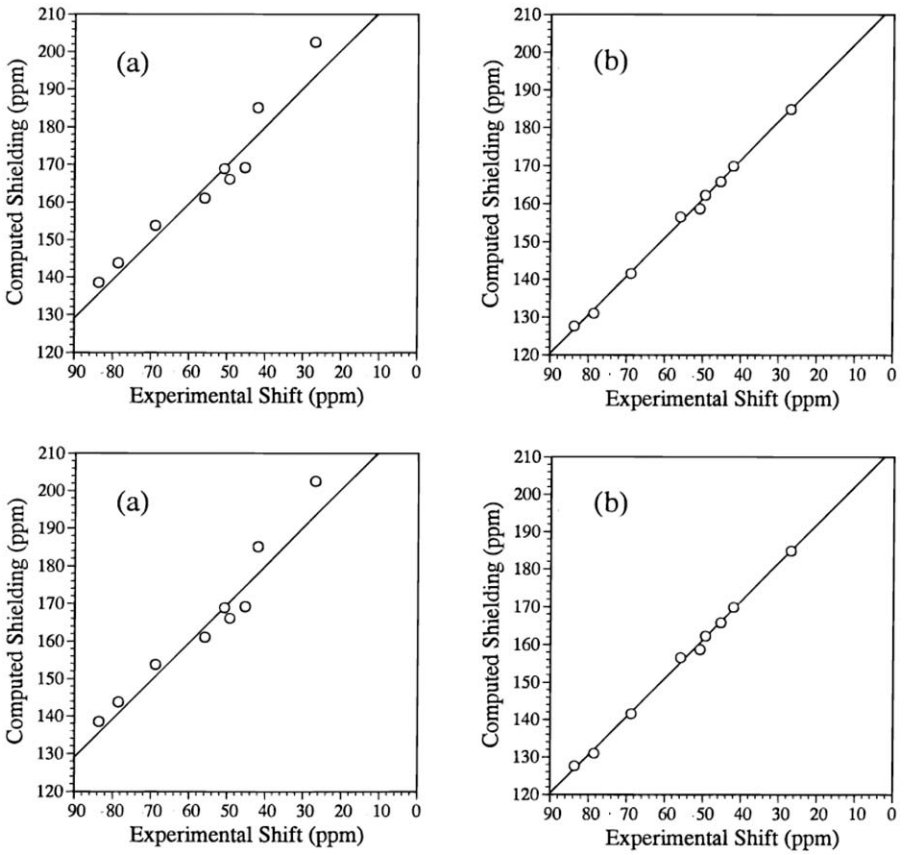

Figure 11 Plot of computed against experimental chemical shifts in pentaerythritol for (a) X-ray atomic positions, with an rms agreement between experiment and theory of 4.45 ppm and (b) neutron diffraction atomic positions with an rms of 0.86 ppm. (Reproduced from Ref. *83* ©American Chemical Society).

chemical shift principal values (PAS), whereas a neutron structure gives an rms of 0.86 ppm. Using the X-ray structure with optimized hydrogen atom positions gives an rms of 1.19 ppm.

In Fig. 11 we have used comparisons of the calculated and experimental chemical shift principal values. Because the chemical shift is a tensorial property this seems quite appropriate, but we also realize that many readers may not be familiar with this concept. Therefore, this is a good place to discuss what it is the PAS (principal axis system) system. The shielding tensor of nucleus A, is a second-rank tensor with nine independent components (*84*). It can be decomposed into antisymmetric and symmetric contributions, $\sigma = \sigma_A + \sigma_S$ (*85*). Generally, the shielding tensor is expressed as the sum of three 0-, 1-, and 2-rank tensors:

$$\sigma = \begin{bmatrix} \sigma_{xx} & \sigma_{xy} & \sigma_{xz} \\ \sigma_{yx} & \sigma_{yy} & \sigma_{yz} \\ \sigma_{zx} & \sigma_{zy} & \sigma_{zz} \end{bmatrix} = \sigma_{iso} \begin{bmatrix} 1 & 0 & 0 \\ 0 & 1 & 0 \\ 0 & 0 & 1 \end{bmatrix} + \begin{bmatrix} 0 & \sigma^A_{xy} & \sigma^A_{xz} \\ \sigma^A_{yx} & 0 & \sigma^A_{yz} \\ \sigma^A_{zx} & \sigma^A_{zy} & 0 \end{bmatrix} + \begin{bmatrix} \Delta_{xx} & \Delta_{xy} & \Delta_{xz} \\ \Delta_{yx} & \Delta_{yy} & \Delta_{yz} \\ \Delta_{zx} & \Delta_{zy} & \Delta_{zz} \end{bmatrix} \quad (23)$$

where the isotropic, antisymmetric, and Δ contributions are:

$$\sigma_{iso} = \frac{1}{3}(\sigma_{xx} + \sigma_{yy} + \sigma_{zz}) \quad (24)$$

$$\sigma^A_{\alpha\beta} = \sigma_{\alpha\beta} - \sigma_{\beta\alpha} \quad (25)$$

$$\Delta_{\alpha\beta} = \frac{1}{2}(\sigma_{\alpha\beta} + \sigma_{\beta\alpha}) - \sigma_{iso}\,\delta_{\alpha\beta} \quad (26)$$

Equation [25] is the antisymmetric part of the shielding tensor, which affects only the relaxation time and not the position of the spectral lines. $\Delta_{\alpha\beta}$ in Eq. [26] is the traceless symmetric component that has five independent components that define the shielding principal axis system (PAS), which is the Cartesian coordinate system in which the Δ tensor is diagonal. If the compound or crystal under study has high symmetry, the PAS systems can be inferred by inspection, but this is not the general case. For instance in the case of the ^{13}C chemical shift tensors of pentaerythritol ($\bar{I}4$ symmetry), which is analyzed in the following section, the *x* axis is along the *a* crystallographic axis, the *y* axis along the *b* axis, and the *z* axis along the *c* axis. The axially-symmetric chemical shift tensor of the central carbon has its principal axis parallel and perpendicular to the 4-fold symmetry *z* axis along the c crystallographic axis. The orientation of the ^{13}C chemical shift tensors of pentaerythritol CH_2OH hydroxymethyl group is typical in that it matches closely to the local bond symmetry of the adjacent atoms. The σ_{33} principal axis is only 4° from the C—O bond, and the σ_{11} principal axis lies only 7.8° from the direction perpendicular to the C—C—O plane.

In many cases, uncertainties in the molecular geometries can produce uncertainties in the calculated shielding values that are larger than the experimental errors and comparable to the error due to approximations used in the calculations, making comparison between calculated and experimental chemical shifts challenging (*86*).

The material presented in this subsection show how sensitive the chemical shifts are to bond lengths and how this can be exploited for structural determinations. *J* couplings are also quite sensitive to bond lengths (*87*), but this sensitivity has not been exploited in structural determination as expensively as for the chemical shifts.

Bond Angles

As with bond lengths, the influence of bond angles on chemical shifts has also been explored, though to a much lesser extent, by using calculations to generate shielding surfaces as a function of angle (*75*). The variations of the first derivative with respect to the angle are less than 1 ppm/° in the amino acid residues mentioned above. In the same study of amino acids mentioned in the previous section, the effect of the backbone bond-angle variations in several different glycine, alanine, and valine residues was also studied (*80*). While the variation with bond length can generally be approximated, by a linear function over a typical bond-length range for a given type of bond, the dependence on bond angles shows a significant curvature even over a ±10° range.

In the case of pentaerythritol (*83*), the C—C—C angle in the solid where the tetrahedral symmetry is not maintained due to distortion from the OH groups was shown to have a dependence on the difference between the perpendicular and parallel components of the central carbon's shift tensor. In calculations of the shielding tensor, this difference showed a 2.7 ppm/° with a linear dependence on the angle; this dependence resulted in a predicted C—C—C angle of 106.6° versus the 107.1° angle measured via neutron diffraction.

The effect of the C—C—X angle (where X= C, O, S) on the isotropic and principal values of the CH_2 carbon was explored for a set of cycloalkanes, cycloalkenes, and heterocyclic compounds (*88*). For the compounds studied, the local symmetry of the CH_2 group

dictates the orientation of the principal axes system of the shielding tensor. Calculations showed one component bisecting the HCH angle, one perpendicular to the HCH plane, and the third perpendicular to the CCX plane (designated δ_{CC}). Experimentally, it was known that in cyclopropane (*8*), with a small CCC angle of 49.8°, the δ_{CC} component is found to be −36 ppm (δ_{33}), while in *n*-eicosane (*89*) with a CCC angle of 110.0°, it was 51 ppm (δ_{11}). The other two components stay in the same rank ordering and show much less variation, such that essentially the entire isotropic difference between these two compounds is reflected in the changes in the δ_{CC} component. In a study of 22 different compounds, some of which even include sizable electronic effects by introducing an O or S atom in the α position relative to the CH_2, these trends were still observed, as shown in Fig. 12. The scatter observed between the lines calculated for cyclopropane and propane is due to other factors affecting the chemical shifts of these compounds, factors which cannot be isolated in the experimental measurements.

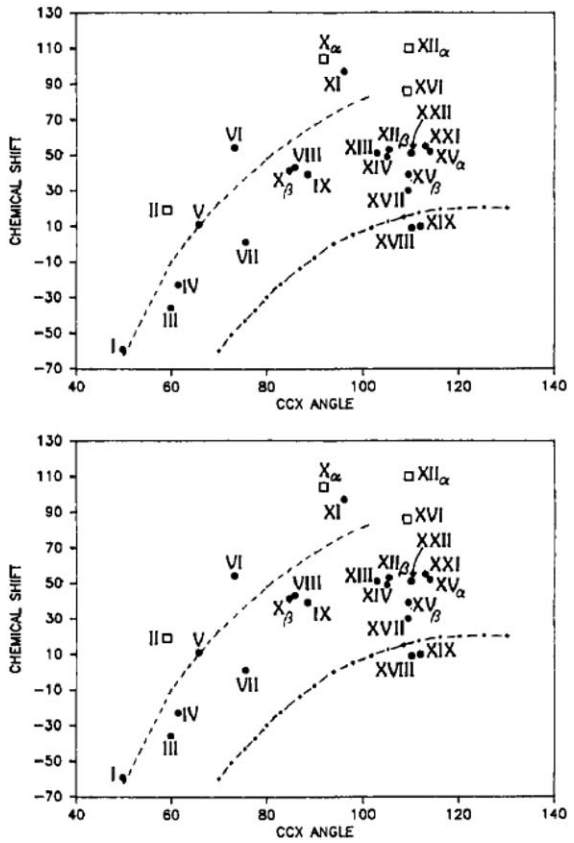

Figure 12 Relationship between δ_{cc} component and CCX angle for a set of 22 CH_2 carbons; cases where X = O are designated as squares. Dashed lines are the calculated angular dependence as a function of CCC angle for the central carbon of cyclopropane (upper) and propane (lower). (Reproduced from Ref. *88* ©American Chemical Society).

The results above show that chemical shifts are sensitive to bond angles and that this sensitivity can be used for molecular structure determination. Much less is known about the dependence on *J* couplings with the bond angles.

Dihedral Angles

A great number of studies on the dependence of chemical shifts on dihedral angles exist in the literature, due mainly to the large role these angles play in determining the overall structure of a molecule. The scope of this article only allows for the mention of a select few, therefore readers are directed to the annual specialist periodical reports on NMR compiled by Jameson and de Dios for a more comprehensive list (*90,91*). It should be noted that, as with bond lengths and bond angles, it is difficult to experimentally isolate only a change in a dihedral angle (*90,91*). Calculations, on the other hand, allow for the study of chemical shift changes due only to the dihedral angle changes as long as the change in the dihedral angle is not accompanied by a re-optimization of the structure of the rest of the molecule.

Paul and Grant (*92*) first studied the so called γ effect, the dependence of the chemical shift on the spatial orientation of a substituent in the γ position using linear regression to separate a number of substituent effects. They found an effect of about 3 ppm between the ^{13}C isotropic chemical shifts of carbons in alkanes and compounds with a γ-carbon in the *gauche* vs. *trans* position. However, due to molecular motion leading to conformational averaging in solution, this is an effect that can be better studied in the solid where the averaging is usually removed. This was done in 1981, when a measurement on powdered syndiotactic polypropene showed two distinct methylene carbon resonances separated by 8.7 ppm, whereas only a single peak was observed in solution (*93*). From the structure it was determined that one of the resonances in the solid was due to a methylene with two *gauche* γ-carbon neighbors, whereas the other was for a methylene with two *trans* γ-carbon neighbors. This effect was also measured by a comparison of the isotropic chemical shifts of the methyl carbon of *cis*- and *trans*-2-butene (*94*), which show a difference of 7 ppm. The tensor components, measured at about 20 K, showed that this difference is all in one component with a 21 ppm difference (27 ppm in *trans*- and 6 ppm in *cis*-butene); calculations show that this component is the one perpendicular to the molecular plane.

In anisole (*95*), by freezing the liquid one gets six carbon aromatic shift tensors as the degeneracy observed in the liquid state between the two *ortho* and two *meta* carbons because conformational averaging is lifted, with the two *ortho* carbons showing an isotropic chemical shift difference of 7.0 ppm and the two *meta* about 1.3 ppm. In the principal components of the shielding tensor, this effect is observed as lower chemical shifts in both the δ_{11} and δ_{33} components of the *ortho* carbon *cis* to the methyl group relative to the *trans ortho* carbon. The effect of methoxy orientation on the ^{13}C chemical shift tensor has also been measured on a number of polysubstituted methoxybenzenes (1,2,3-tri, 1,4-di, and 1,3,5-tri) via single-crystal NMR experiments (*96*), with similar results.

Calculations have been used to explore the dihedral angle defining the orientation of the OH hydrogen in several compounds (*82,97–99*). In a single crystal study on *meso*-erythritol (1,2,3,4-butanetetrol) (*82*), it was found, as depicted in Fig. 13, that the variation of the chemical shift in the principal components of C_1 with respect to the dihedral angle of the C_1 hydroxy H relative to the carbon chain are larger than for the isotropic chemical shifts. As can be observed from this figure, neither the isotropic chemical shifts nor the δ_{33} components are sensitive to the dihedral angle, whereas the effects on the remaining two components mirror each other. Plots such as this can be generated and used to predict the dihedral angle.

Another case where dihedral angles play an important role is in conformational polymorphism; one example is the so called "ROY" polymorphs of

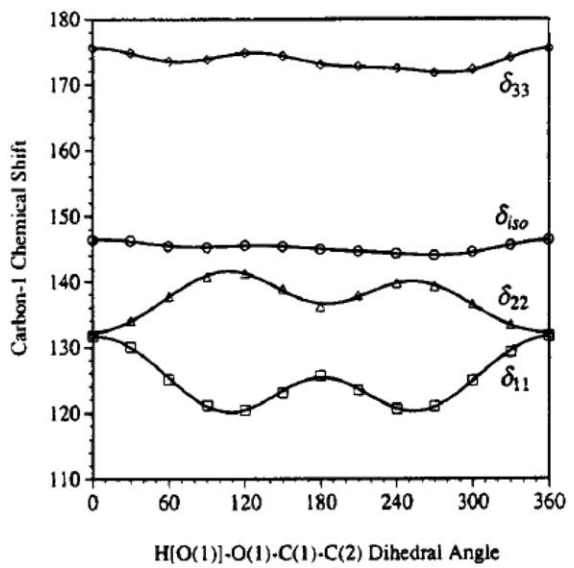

Figure 13 Principal value and isotropic chemical shifts of C_1 of mesoerythritol as a function of the H—O—C_1—C_2 dihedral angle. (Reproduced from Ref. *82*.)

5-methyl-2–3-thiophenecarbonitrile (*100,101*). The three polymorphs, shown in Fig. 14, have colors of red, orange, and yellow while differing mainly in the dihedral angle between the phenyl and thiophene ring. Calculations of the shielding tensors were completed as a function of this dihedral angle; from a least-squares fit between the experimental ^{13}C and ^{15}N principal values of the three forms and these calculated values, predicted dihedral angles were obtained for each form. The plot of the variation of the fit with angle and a comparison with the X-ray dihedral angle is shown in Fig. 14.

The same variation in dihedral angles that gives rise to conformational polymorphism can also be observed in the cases where independent molecules per asymmetric unit differ only by conformation. This has been recently observed by Harris et al. in a study of the mod II polymorphic form of oxybuprocaine hydrochloride (*102*). This molecule exhibits a high degree of conformational flexibility, with one of the molecules in the asymmetric unit being "stretched out" while the second is in a "bent" conformation. This leads to differences in most of the carbon chemical shifts between the two forms, with the isotropic chemical shifts showing differences of up to 4.2 ppm. It can also be noted that one of the conformational changes observed is the γ effect mentioned earlier due to a gauche arrangement of substituents.

The use of chemical shifts to determine molecular conformation is perhaps most widely applied in the study of the structure of amino acids, peptides, and proteins, both in solution and in the solid state. This field has been extensively reviewed (*103–105*). While there has also been some effort on the use of ^{15}N (*106*) and ^{1}H chemical shifts (*107*), most of the work is focused on using ^{13}C chemical shift parameters (using either isotropic shifts, CSA, or tensor components) of the C^{α} and C^{β} carbons in the determination of the Ramachandran angles φ,ψ to establish the backbone structure and the determination of the various χ angles to determine the orientation of the side chains (*108,109*). Calculations of the relationship of isotropic chemical shifts to the φ,ψ angles have also been used for further refinement of structures obtained from solution-state NMR methods.

Oldfield and coworkers have published a number of studies on the relationship between structure and chemical shifts in peptide fragments, including the effects of the backbone and side chain dihedral angles (*76,110*). The work of his group in this field, discussed below, has demonstrated the dominance of the local nature of shielding, in suggesting that calculations on models of individual amino acids can be used to predict the shifts in larger peptides (*111–114*). In a typical study, model

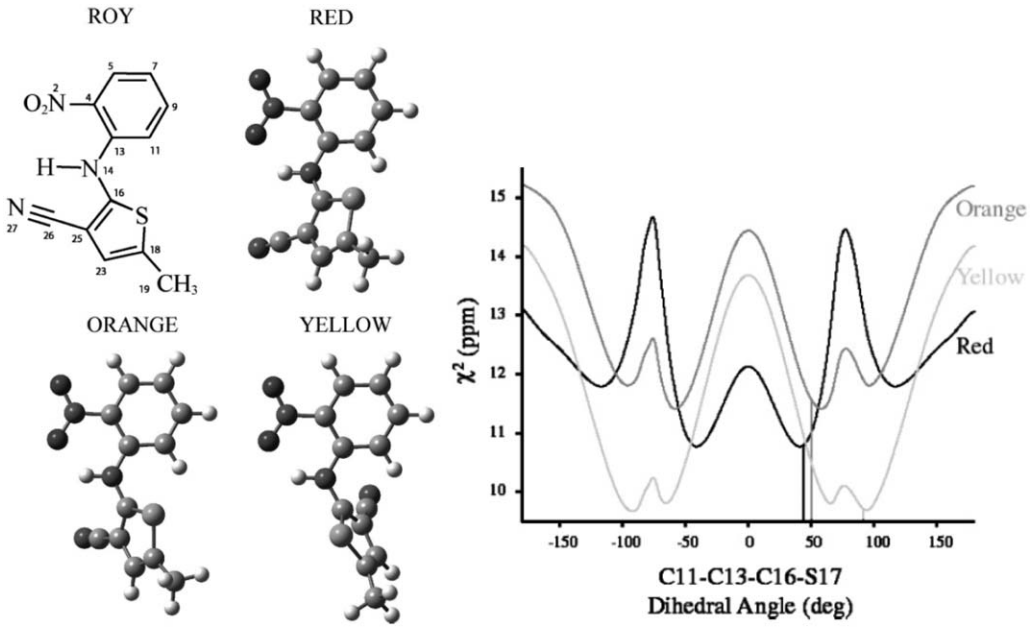

Figure 14 ROY polymorphs and chemical structure showing that variation between the polymorphs occurs in the dihedral angle C11—C13—C16—S17. The variation of the least-squares comparison (χ^2) of ^{13}C- and ^{15}N-NMR data as a function of this angle; X-ray angles are marked as vertical lines. (Reproduced from Ref. *101* ©American Chemical Society).

fragments are used for an amino acid in a peptide. The fragments typically consist of an *N*-formyl amino acid amide. Studies have shown that the effects of truncation and capping on the calculated chemical shift values relative to the experimentally measured values are minimal. In addition, it has also been shown that the C^{α} carbon isotropic shifts in these compounds are dominated by the effect of the torsion angles, suggesting that changes in other geometrical factors such as bond length and angles that may accompany the change of the dihedral angle may be neglected. Both of these observations support the generation of shielding surfaces based on only changes in the φ, ψ angles.

Strohmeier and Grant (*115*) applied Oldfield's methodology, using the principal values of both the ^{13}C and the ^{15}N chemical shift tensors to determine the backbone conformation of melanostatin, L-Pro-L-Leu-Gly amide. The C^{α} tensor components on capped fragments were used to establish the backbone φ, ψ angles; these surfaces were then refined with information on the orientation of the C^{α} components relative to the C—N bond derived from ^{13}C–^{14}N coupling and the C^{β} shift components. This work also reported the X-ray structure of this compound to allow for a comparison.

The application of chemical shifts to study conformation in biological systems is not limited to only peptides and proteins—it has also been used in the analyses of nucleic acids (*116–118*), nucleosides/nucleotides (*119*), and polysaccharides (*120*). For polysaccharides, the angles describing the glycosidic linkages have been well correlated to the isotropic ^{13}C chemical shifts of the carbons involved in the linkage. Sergeyev and Moyna (*121*) have calculated chemical shielding surfaces for oligosaccharides and used the surfaces along with the experimental solid-state isotropic ^{13}C chemical shifts and NMR pseudopotential energy surfaces as constraints to model the linkage angles; results were within 10° from known X-ray structures.

Until a few years ago (*59*), NMR stereochemical analyses were mainly based on long range couplings, occupying prominent places were the Karplus equation (*122,123*) and its generalization (*124*) for ^{3}J(HH) couplings, Karplus-like relationships for three-bond couplings between different isotopic species, and Schaefer's "J method" for studying side chain conformations in aryl compounds (*122,125*). In general, the main idea is to obtain relationships between a given type of coupling constant and some structural parameter. Such relationships are obtained either theoretically or empirically. Such possibility was greatly enhanced owing to the important advances that also took place on experimental techniques, both for obtaining isotopic enriched samples, especially in ^{13}C and/or ^{15}N, and with the development of special techniques to detect different couplings and enhance their resolution.

The angular dependence of ^{3}J(HH) in ethane, fluoro ethane, and 1-1-difluoroethane was explored (*126*) employing different basis sets at the HF RPA level.

The major contribution to these calculated couplings is given by the FC term. Dependence of Karplus-type equation parameters for ^3J(HH) on substituents were calculated by San Fabián et al. (*127*) in monosubstituted ethanes, CH_3CH_2X (X=CH_3, NH_2, OH, and F) employing the 6–31G** basis set at the HF RPA level for the FC term. Calculated substituent effects, ΔJ^X, increase when increasing the substituent electronegativity. Substituent effects on ^3J(HH), $\Delta^3J^X_{Me}$, were also calculated by Guilleme et al. (*128*) (Fig. 15) in monosubstituted and 1,1-disubstituted ethanes, with substituents containing atoms from the 2nd to the 5th rows of the periodic table. From experimental and calculated data sets they concluded that experimental couplings, $^3JMe^X$, as well as calculated substituent effects of monosubstituted ethanes follow a quadratic dependence on the relative electronegativity, $\Delta\chi_x = \chi_x - \chi_H$, of the substituent directly bonded to the ethanic fragment, that is the α atom. β-Hydrogen effects on vicinal ^3J(HH) couplings were studied employing *ab initio* methods in CH_3CH_3X (X=CH_3, NH_2 and OH) (*129*).

Schaefer et al. (*130*) studied departures from the Karplus-type relationship ("Barfield effect") to determine the ring pucker in 2-phenyl-1,3-dithiane. The dependence of the ^3J(HH) Karplus equation on the internal C—C—H angles was given in mathematical

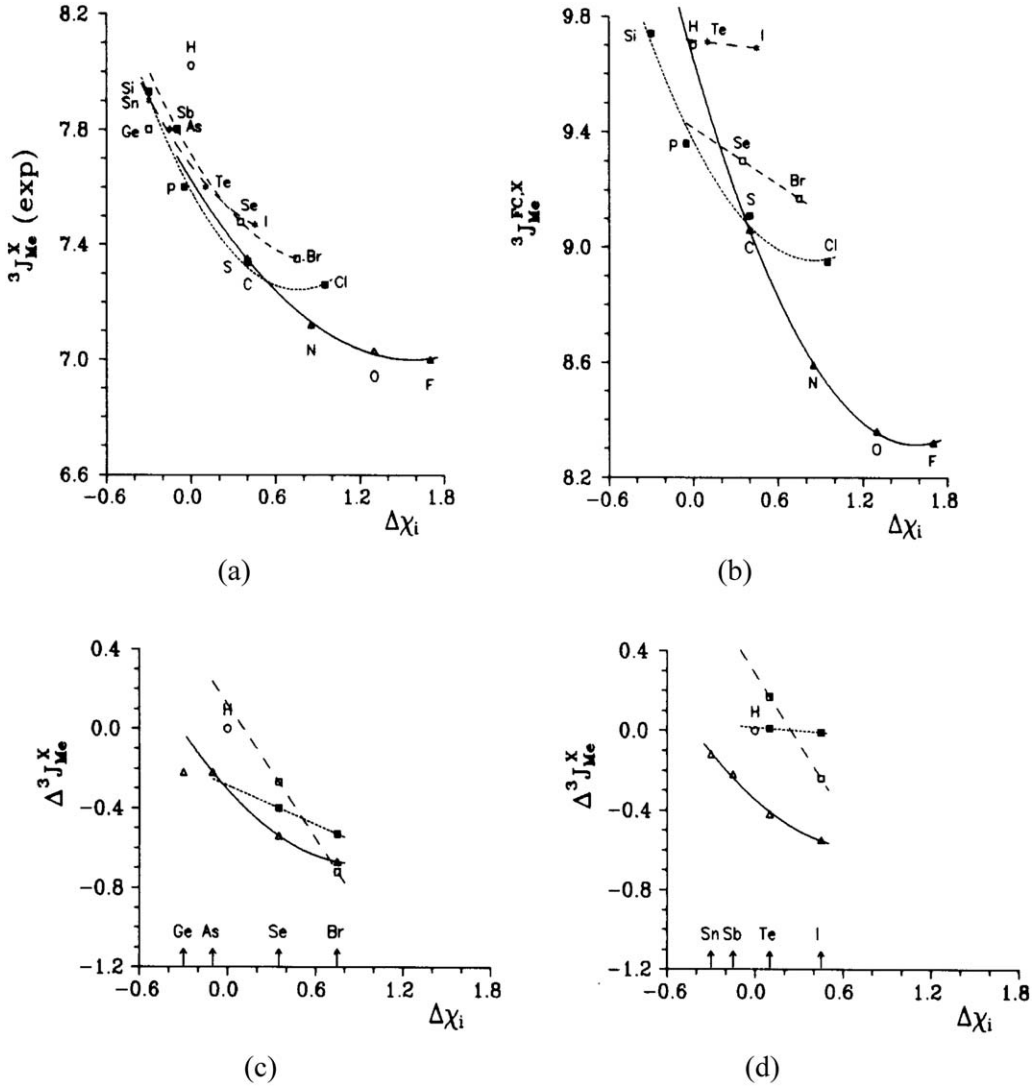

Figure 15 Experimental and calculated individual substituent effects $\Delta^3J^X_{Me}$, in hertz, as a function of the relative electronegativity Δχx, where α atoms of substituents belong to the second (a), third (b), fourth (c), and fifth (d) rows of the periodic table.: (—), (Δ), experimental values; (----), (□), calculated values with standard geometry; (. . .), (■), calculated values with optimized geometry. (Reproduced from Ref. *128* ©Taylor & Francis).

form by Barfield and Smith (*131*), who also recalculated the coefficients using new experimental data for dihedral angles close to 180° in an sp^3–sp^3 system (*132*).

^3J(HH) couplings through the HNCH$^\alpha$ pathway were accurately determined in ^{15}N-enriched proteins and the corresponding Karplus equation, Eq. [27], was parameterized using residues where the backbone angle is known (*133*), giving, $A = 6.51$ Hz; $B = -1.76$ Hz, and $C = 1.60$ Hz with a rms deviation of 0.73 Hz.

$$^3J(\mathrm{H^N H^a}) = A \cdot \cos^2(\varphi - 60^\circ) + B \cdot \cos(\varphi - 60^\circ) + C \quad (27)$$

Experimental ^3J(HH) couplings in metallapentacyles N—C—C—O—M (M=Rh(III) and Ir(III) were used to parameterize a Karplus equation for a H—C(sp^3)—N(sp^3)—H pathway (*134*). The plot of ^3J(HH) against the torsion angle φ (H-N-C-H) and the curve adjusted to Karplus Eq. [27] is shown in Fig. 16 (*134*).

$$^3J(\mathrm{H,H}) = 8.9\ \cos^2\varphi - 1.0\ \cos\varphi + 0.8 \quad (28)$$

To take into account the conformational flexibility, when studying the structure of different biological compounds, the use of an adequate force field is required. Some of them were compared in carbohydrates to assess how well several kinds of experimental data are reproduced (*135*). Among them, ^3J couplings were considered for H—C—C—H and C—O—C—H coupling pathways using the equations given by Haasnoot and coworkers (*136*) and Tvaroska et al. (*137*), respectively. ^3J(CH) couplings were used to carry out a conformational analysis of oligosaccharides (*138*) and such couplings were also used as probes to detect solvent effects on their conformations. Calculations of vicinal carbon–proton coupling in propane, 1-fluoropropane, and 2-fluoropropane and their angular dependence were carried out by San Fabián et al. (*139*) employing standard Gaussian-type basis sets enriched with tight s functions on C and H centers, the experimental angular dependence and substituent effects for these couplings in larger compounds were successfully reproduced.

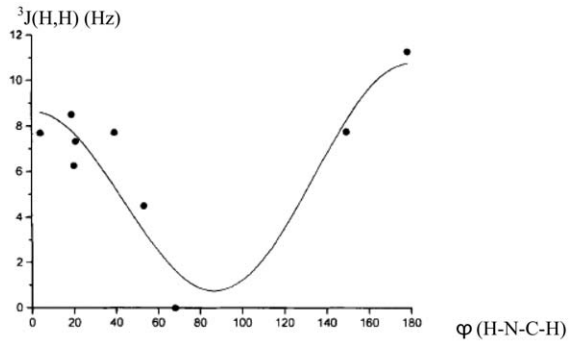

Figure 16 Karplus type plot: ^3J(H,H) as function of the φ (H—N—C—H) pathway. (Reproduced form Ref. *134* ©John Wiley & Sons.

Wang and Bax (*140*) reparametrized the Karplus equation for ^3J(H$^\alpha$N) and ^3J(H$^\mathrm{N}$C') (*137*), and ^3J(H$^\mathrm{N}$H$^\alpha$) and ^3J(H$^\alpha$C') for peptides using uniformly ^{13}C/^{15}N-enriched human ubiquitin (*141*).

Stereochemical aspects of ^3J(CH) couplings through a H—C—C=C pathway were discussed in a set of rigid compounds, (*142*) and differences between *cis* and *trans* ^3J(CH) couplings through a vinylic moiety, H—C=C—C were discussed in propenoic acids (*143*). ^3J(CC) Karplus-type equations for a C—O—C—C pathways were presented (*144*).

This subsection shows how useful and universal is the use of both experimental measurement and calculations of *J* couplings and chemical shifts to determine the dihedral angles in a great variety of molecules. Certainly, the determination of dihedral angles by NMR aided techniques is one of the most common applications of NMR for structure elucidation and while some of the references given here are quite old, still this early methods are widely used and of proven utility.

Packing and Symmetry

In most cases there are no or only very minor differences between the isotropic chemical shifts measured in solution (in a non-polar solvent) versus those measured in the solid state either in a MAS spectrum or from the average of a measurement of the principal values of the chemical shift tensor (*145*). When this is the case, it is an indication that intermolecular effects are probably not an important factor in the system under study and that there are no crystal effects complicating the interpretation of the SSNMR (Solid State NMR) spectra. Often in these cases there is also good agreement (typically within 5 ppm for the principal values) between the experimental chemical shift values and the results of calculations done on a single isolated molecule. However, there are many examples in the literature where substantial differences are measured between solution and solid-state chemical shifts and/or between experimental solid-state data and single molecule theoretical measurements. In some cases these differences in the isotropic chemical shift values are of such magnitude that duplication of lines may be observed in the SSNMR spectra. When such differences are observed one must look to the structure of the molecule and its local environment for reasons to explain the differences. Some of the differences are due to changes in the

molecule itself (structure and/or dynamics) upon going from solution/liquid to solid, while others are due to strong intermolecular interactions in the solid state. The main contributions to solid state effects are described in a recent review (*146*) and they include:

- Conformational and tautomeric averaging
- Crystal symmetry
- Multiple molecules per asymmetric unit
- Presence of polymorphs
- Multiple solid state phases
- Electrostatic effects
- Hydrogen bonding
- Magnetic effects

While the experimental measurements can provide unequivocal evidence of the existence of solid state effects on chemical shifts, the experiments alone seldom can provide conclusive information on their chemical and/or structural origins. Theoretical and computational methods play a fundamental role in interpreting the experimental results and provide insight on the physical origin of the solid state effects. This is possible because the calculations are able to test a variety of models, each of which can selectively include different plausible mechanisms that may be responsible for the solid state effect observed in the chemical shifts.

The theoretical methods available to take into account intermolecular interactions can be classified into mainly two categories: those that represent the intermolecular interactions by an electric or magnetic field that mimics the interactions generated by the rest of the molecules in the crystal and those that explicitly treat the neighboring molecules. Most of the methods in the first category use either a finite distribution of charges or multipoles to represent the electric field generated by the environment (*104,147–154*). Recently it has been shown that it is possible to observe purely magnetic intermolecular effects (*90*) and in this case the use of nucleus independent chemical shielding (*155–157*) calculations has been used to take into account these effects (*158*). The second category of methods available treats the neighboring molecules explicitly in the quantum mechanical calculations of the chemical shielding (*104,147–154*). For a number of years the explicit representation was accomplished by including a finite number of neighboring molecules in the calculations. This approach is usually described as the "cluster model." The greatest disadvantage of the "cluster model" methods is that their computational costs increases rapidly with the number of neighboring molecules included in the calculations. To avoid this problem a number of combinations of cluster and electrostatic models have been used over the years; in these hybrid models the closest neighbors are explicitly represented and the more remote ones are replaced by an approximate field.

In recent years several research groups have reported new theories that allow the calculation of shielding in systems with periodic boundary conditions (PBC). These theories eliminate the need of using the inherent approximations of the cluster and electrostatic methods by including in the calculations all the interactions arising from the crystal field. Sebastiani and Parrinello (*159–163*) implemented their method in the popular CPMD program (*164*) using localized Wannier orbitals and a periodic pseudo position operator with a saw-tooth shape. This method can be used to calculate shieldings in both isolated and full periodic systems. A similar theory was presented by Mauri et al. (*165*) in which the problems associated with the lack of definition of the position operator in periodic systems has been resolved by using a modulated external magnetic field; they calculate the shielding by numerical differentiation of the values calculated for two small, but not zero, wave vectors. This method, as well as the one from Sebastiani, has been implemented using pseudo potentials and therefore cannot be taken into consideration the contribution of the inner shells. This approximation can be problematic for non first row nuclei and in a subsequent paper (*166*), Pickard and Mauri introduced the Gauge Including Projector Augmented Wave (GIPAW) method that formally includes the contribution of the core electrons when using pseudo potentials. Numerous applications using this method have been presented (*165–175*). Recently, the same methods have been implemented in the Quantum Espresso code (*176*). To the authors knowledge there is no software available to calculate *J* couplings using PBC.

In conclusion, the computational methods have advanced to the point that there is widely available software that can predict with great accuracy the chemical shifts in solid state and by comparison of calculation in the solid state and the isolated molecule is possible to provide a rationalization for experimental observations of solid state effects.

NMR CRYSTALLOGRAPHY

The recent methodological advances described in the sections above and the increasing experimental capabilities for high resolution SSNMR have been used to establish the field of NMR crystallography (*177–179*), which capitalize in the extremely high sensitivity of the NMR chemical shifts observed many years ago (*86*) and by combining new experimental and computational methodologies has produced a semi-structured approach to solve molecular and crystal structures

using either solely SSNMR and/or conjunction with powder diffraction techniques. In general, these approaches are not as powerful as conventional X-ray or neutron diffraction, but provide very useful alternatives when single crystals are not available.

The examples discussed above give a clear indication of the great potential for using NMR chemical shifts for structure elucidation. The strong sensitivity of the chemical shifts to molecular structure (*86*) is the basic property that makes this possible. The examples also show that the relationship between structure and chemical shift is not simple. In contrast with the simple relationship between structure and NOEs given by the $1/r^6$ dependence on the distance between nuclei or even the reciprocal lattice relationship between X-ray or neutron diffraction patterns and molecular structure, the relationship between chemical shift and molecular or crystal structure is mediated by the complex quantum mechanical machinery presented in previous sections of this review. Consequently, until recently most applications used *ad hoc* approaches like those described above. In recent years, we have seen a consistent effort by several research groups to develop systematic ways to obtain molecular and crystal structures using NMR chemical shifts. This emerging field has been named "NMR Crystallography" (*179*). While it is recognized that solid-state NMR cannot be competitive with diffraction methods when single crystals are available, the methodology has been shown to be competitive with powder diffraction and other techniques commonly used when single crystals are not available. Although even when single crystals are available, SSNMR techniques can be very competitive with X-ray diffraction in locating H atoms (*82*). In this section, we provide a brief account of some of the advances in this field; a comprehensive report on the state of the art of the field was provided recently (*178,179*).

Using the principles of NMR crystallography, Meejoo et al. (*180*) studied the structure of the β-polymorph of (*E*)-4-formylcinnamic acid. The structure refined as an ordered structure using the powder diffraction spectra led to a high quality structure, but the high resolution solid-state ^{13}C-NMR spectrum of this material showed evidence of disorder of the formyl group. When using the information of the disorder of the formyl group into the refinement, the Rietveld quality factors, R_{wp}, improved from $R_{wp} = 3.27\%$ to $R_{wp} = 2.87\%$.

Witter et al. (*181*) studied the ^{13}C chemical shift resonances of bacterial cellulose by solid-state NMR and performed a constrained crystal structure refinement. The solid-state NMR assignments of the ^{13}C resonances of bacterial cellulose *I*α were reinvestigated by INADEQUATE experiments on uniformly ^{13}C-enriched samples from *Acetobacter xylinum*. The authors determined the principal components of the chemical shift tensors of each ^{13}C labeled site from a 2D iso–aniso RAI (recoupling of anisotropy information) spectrum acquired at a MAS speed of 10 kHz. On the basis of these NMR data, the crystal structure of cellulose *I*α was refined using the ^{13}C chemical shifts as target functions. Starting off with the coordinates derived from neutron scattering (*182*) and using molecular dynamics simulations, a total of 800 structures were selected for further consideration. These structures were subsequently optimized within the given isotropic chemical shift constraints and applying crystallographic boundary conditions in the shielding calculations. The resulting four model structures that best fit the NMR data were then assessed by simulating the chemical shift tensors, using the bond polarization theory, and comparing these values with the experimental CSA information obtained by RAI spectra. The earlier neutron diffraction study had reported two possible occupation schemes for the hydrogen-bonded hydroxyl groups that connect the cellulose chains. From these two possibilities, the NMR results single out one pattern as the most probable structure.

Grant and coworkers have presented a combined solid-state NMR and synchrotron X-ray diffraction powder study on the structure of the antioxidant (+)-catechin 4,5-hydrate (*183*). As in the case of cellulose there is a marked improvement in the agreement between calculated and experimental chemical shifts upon refining the crystal structure using the NMR information.

Following the previous studies of solid-state polymorphism in 10-deacetyl baccatin III (*98*), the Grant group presented the structural characterization of a new anhydrous polymorph of paclitaxel based on solid-state NMR and X-ray powder diffraction methods (*184*). The three-dimensional structure of this unique polymorph of the anticancer drug paclitaxel (Taxol®) was established using solid-state NMR tensor (^{13}C and ^{15}N) and heteronuclear correlation (^{1}H–^{13}C) data. The polymorph has two molecules per asymmetric unit ($Z = 2$) and is thus the first conformational characterization with $Z > 1$ determined solely by SSNMR. Experimental data were correlated with structure through a series of computational models that extensively sampled all possible conformations of the molecules. For each computational model, corresponding tensor values were computed to supply comparisons with experimental information, which, in turn, establishes the paclitaxel's new polymorph structure. Heteronuclear correlation data at 13 key positions provided shift assignments into the asymmetric unit for each comparison. The two distinct molecules of the asymmetric unit

possess nearly identical baccatin III moieties with matching conformations of the C10 acetyl moiety and, specifically, the torsion angle formed by the C30—O—C10—C9 atoms. Additionally, both are found to exhibit an extended conformation of the phenylisoserine side chain at C13 with notable differences in the dihedral angles centered on the rotation axes of O—C13, C20—C10, and C30—C20.

While the methods in which NMR crystallography are still evolving, this is already an established field widely recognized as a valid and powerful for structure elucidation. As on November 2013, a Scopus (http://www.scopus.com) search of the phrase "NMR crystallography" produced more than 80 citations.

SOFTWARE AND HARDWARE CONSIDERATIONS

Significant shielding and *J* coupling calculations can be done using hardware and software commonly available in most structural chemistry labs. With this in mind, it is important to provide a short account of the software available and the hardware necessary for NMR shielding calculations. Here we describe, in alphabetical order, several of the most common software packages that can be used to calculate shieldings. The reader should notice that the software list is not comprehensive and that at the time of writing this review the calculation of NMR properties is becoming a standard feature of most QM packages.

ACESII (http://www.qtp.ufl.edu/ACES/): ACES II uses the coupled-cluster approach to handle electron correlations in atoms and molecules. This approach sums entire select classes of Feynman diagrams in many body theory to provide a good approximation of the correlation energy. It has been used successfully on small molecules in computing ground state electronic properties and excited states. It provides capabilities to evaluate analytically NMR shielding tensors at the SCF and MBPT(*2*) levels using gauge-including atomic orbitals (GIAOs) to ensure exact gauge-invariance.

ADF (http://www.scm.com/): The Amsterdam Density Functional Package is being developed at the well-known theoretical chemistry groups of Profs. Baerends, Ziegler, Snijders, and by several other scientists worldwide. This package can calculate NMR chemical shifts and spin–spin couplings using density functional theory, including relativistic corrections and all-electron basis sets for the whole periodic table.

CADPAC (http://www-theor.ch.cam.ac.uk/software/cadpac.html): NMR shieldings can be calculated using the LORG algorithm for the DFT and HF electronic approximations.

CASTEP (DFT/GIPAW) (http://www.castep.org/): This software has implemented the GIPAW method presented by Mauri and coworkers (*165,166,185*). CASTEP uses density functional perturbation theory and the GIPAW method to compute magnetic shielding (chemical shift) tensors in solids and molecules (*165,166,185*). CASTEP uses density functional perturbation theory and the GIPAW method to compute magnetic shielding (chemical shift) tensors in solids and molecules. It is also possible to compute electric field gradient tensors (EFG). A development version of the code can compute *J*-coupling tensors.

CPMD (http://www.cpmd.org/): The Carr-Parrinelo Molecular Dynamics code has implemented the theory to calculate NMR shielding for periodic system reported by Sebastiani and Parrinello.

DALTON (http://www.kjemi.uio.no/software/dalton/dalton.html): This software can calculate NMR properties (both magnetizabilities, nuclear shieldings, and all contributions to nuclear spin–spin coupling constants) and EPR properties (electronic g-tensor, hyperfine coupling tensor, and zero-field splitting tensor) at the HF/DFT/MCSCF levels of approximation.

deMon (http://www.demon-software.com/public_html/index.html): This software has implemented the calculation of NMR shieldings using the DFT approximation within the SOS scheme described by Malkin et al. (*186*).

GaussianXY (http://www.gaussian.com/): This software package can be used to calculate shieldings and *J* couplings and it is available commercially. Using the framework of the CDFT (Coupled DFT) perturbation theory, Gaussian implemented the calculation of shielding tensors in the popular Gaussian suite of programs (*187*). This implementation makes use of the techniques previously developed by Pulay and coworkers (*188–190*) to efficiently calculate the complex two electron integrals necessary to implement the GIAO formulation (*188–190*). A number of additional methods to calculate shieldings have also been implemented in the Gaussian suite of programs in recent years. These include HF, DFT, and MP2 electronic approximations as well as single origin, GIAO, IGAIM, and CSGT methods to deal with the gauge origin-dependence problem. The accuracy of calculations is highly dependent on the basis set used. While the standard basis sets of quantum chemistry are well developed for valence electrons, a more sophisticated description of the electron density closer to the nuclei is needed for predicting the Fermi contact (FC) term (often the spin–spin coupling constants' largest component). Researchers at Gaussian, Inc. have explored this problem in depth and have developed modified basis sets suitable for modeling these quantities within a

DFT framework; their results are summarized below. When requested, Gaussian will automatically perform a two-step calculation for NMR spin–spin coupling, using the standard basis set for the general calculation and the corresponding modified basis set for the FC term.

Jaguar (http://www.schrodinger.com/products/14/7/): It allows the calculation of NMR shielding constants in gas phase and solution using HF, DFT, and other highly correlated methods.

NWChem (http://www.nwchem-sw.org/index.php/Main_Page): This software has implemented the calculation of NMR shielding (GIAO method) for the HF electronic approximation using the coupled Hartree-Fock scheme and DFT methods.

PQS (http://www.pqs-chem.com/): This software was known in the past as the Texas program by Pulay and Hinton (*189*). Nuclear magnetic shieldings for closed-shell HF and DFT wavefunctions can be calculated for common gauge and GIAO gauge choices. The program has been parallelized to run in computational clusters.

Quantum Espresso (http://www.quantum-espresso.org/): Has implemented DFT/GIPAW calculations using the GIPAW method (*165,166,185*). This code is available as an open source license (*176*).

Modest shielding calculations in systems with up to 10–20 non-hydrogen atoms and using a few hundreds of basis functions can be done in reasonable time using typical desktop computers. While these calculations cannot be done in an interactive fashion, overnight runs for each shielding calculation are a reasonable expectation. If a geometry optimization of the molecule is necessary before performing the shielding calculation, this time may increase significantly depending on the quality and magnitude of the geometry optimization needed. Much larger calculations are more suitable for large clusters or other parallel supercomputer systems. From the exhaustive, but perhaps not comprehensive and always evolving list of available software it is apparent that non NMR specialist can secure the tools necessary for using high resolution NMR data in structure elucidation at a modest cost that is within the typical budget of moderate to large research organizations. Even using open source software may it be possible for small teaching colleges to introduce the basic concepts and provide practical exercises to illustrate the concepts discussed in this article to upper division undergraduate students or first year graduate students.

CONCLUSIONS

This article provides a comprehensive review of the different ways in which the measurement of high resolution NMR parameters, both in solution and in solid state, can be combined to extract important structural information about molecules and their environment. While many of these techniques have been available from a long time the advances in both instrumentation and computational methods and capabilities are making them more common and easily accessible to the average researcher interested in molecular structure determination. In spite of the advances reported here, the use of this techniques requires substantial know how and adaptation to each application. This is apparent from this review, in which we have demonstrated the use of different techniques based on examples collected from the literature. This contrasts with the maturity observed in other methods commonly used for structure determination based on diffraction methods, for which there are very well defined and standard practices for data acquisition, processing, and analysis. With the advent of the new field of NMR crystallography, we expect that in a no distant future the field will mature to the point that integrated NMR crystallography pipelines, as robust as those for X-ray diffraction, will develop and make widely available. In the mean time we believe that this article provides a substantial number of examples that can guide new investigators on how to construct pipelines targeted to their specific structural problems.

REFERENCES

1. Lippens G, Jeener J. 2001. The dipolar interaction under all angles. Concepts Magn Reson A 13:8–18.
2. Levitt MH. 2001. Spin Dynamics. Chichester: Wiley.
3. Duer MJ. 2002. Solid-State NMR Spectroscopy. Oxford: Blackwell Science. pp 46-56.
4. Anet FAL, Bourn AJR, Carter P, Winstein S. 1965. Nuclear magnetic resonance spectral assignments from nuclear overhauser effects. J Am Chem Soc 87: 5250–5251.
5. Alderman DW, Solum MS, Grant DM. 1986. Methods for analyzing spectroscopic line shapes NMR solid powder patterns. J Chem Phys 84:3717–3725.
6. Eichele K, Wasylishen RE, Schurko RW, Burford N, Whitla WA. 1996. An unusually large value of 1J(31P,31P) for a solid triphenylphosphine phosphadiazonium cationic complex: determination of the sign of *J* from 2D spin-echo experiments. Can J Chem 74:2372–2377.
7. Griffiths JM, Griffiths RG. 1993. Nuclear magnetic resonance methods for measuring dipolar couplings in rotating solids. Anal Chim Acta 283:1081–1101.
8. Zilm KW, Beeler AJ, Grant DM, Michl, J, ChouTC, Allred EL. 1981. Carbon-13 magnetic resonance dipolar spectroscopy. Orientation of the chemical shift tensor in cyclopropane. J Am Chem Soc 103:2119–2120.

9. Browna SP, Emsley L. 2004. The 2D MAS NMR spin-echo experiment: the determination of 13C–13C *J* couplings in a solid-state cellulose sample. J Magn Reson 171:43–47.
10. Grage SL, Watts A. 2007. Applications of REDOR for distance meassurements in biological solids. Ann Rep Nucl Magn Reson Spectrosc 60:191–228.
11. Schnell I. 2004. Dipolar recoupling in fast-MAS solid state NMR spectroscopy. Prog NMR Spectrosc 45: 145–207.
12. Andrew ER, Bradbury A, Eades RG. 1959. Removal of dipolar broadening of nuclear magnetic resonance spectra of solids by specimen rotation. Nature 183: 1802–1803.
13. Lowe IJ. 1959. Free induction decays of rotating solids. Phys Rev Lett 2:285–287.
14. Jaroniec CP. 2009. Dipolar recoupling: heteronuclear. In: Harris RK, Duer MJ, eds. NMR Crystallography. Chichester: Wiley. pp 137–161.
15. Guillon T, Scharfer J. 1989. Rotational-echo double-resonance NMR. J Magn Reson 81:196–200.
16. Gullion T, Schaefer J. 1989. Detection of weak heteronuclear dipolar coupling by rotational-echo double-resonance nuclear magnetic resonance. Adv Magn Reson 13:57–83.
17. Raleigh DP, Levitt MH, Griffin RG. 1988. Rotational resonance in solid state NMR. Chem Phys Lett 146: 71–76.
18. Levitt MH, Raleigh DP, Creuzet F, Griffin RG. 1990. Theory and simulations of homonuclear spin pair systems in rotating solids. J Chem Phys 92:6347–6364.
19. McDowell LM, Schaefer J. 1996. High resolution NMR of biological solids. Curr Opin Struct Biol 6:624–629.
20. Oas TG, Griffin RG, Levitt MH. 1988. Rotary resonance recoupling of dipolar interactions in magic angle spinning NMR spectroscopy. J Chem Phys 89:692–695.
21. Levitt MH, Oas TG, Griffin RG. 1988. Rotary resonance recoupling in heteronuclear spin pair systems. Isr J Chem 28:271–282.
22. Fu R, Smith SA, Bondenhausen G. 1997. Recoupling of heteronuclear dipolar interactions in solid state magic-angle spinning NMR by simulatneous frequency and amplitude modulation. Chem Phys Lett 272:361–369.
23. Takegoshi K, Takeda K, Terao T. 1996. Modulatory resonance recoupling of heteronuclear dipolar interaction under magic angle spinning. Chem Phys Lett 260:331–335.
24. Duer MJ. 1999. Solid state NMR. Physical organometallic chemistry. In: Solid State Organometallic Chemistry. Duer MJ, ed. London: Wiley. pp 227–277.
25. Tycko R, Dabbagh G. 1990. Measurement of dipole-dipole couplings in magic angle spinning NMR. Chem Phys Lett 173:461–465.
26. Haeberlen U, Wangh JS. 1968. Coherent averaging effects in magnetic resonance. Phys Rev 175:453–467.
27. Tycko R. 2009. Coupling interactions. In: Harris RK, Duer MJ, eds. NMR Crystallography. Chichester: Wiley; 164–176.
28. Nielsen NC, Bildsoe H, Jakobsen HB, Levitt HM. 1994. Double-quantum homonuclear rotatory resoanance: efficient recovery in magic-angle spinning nuclear magnetic resonance. J Chem Phys 101:1805–1812.
29. Gullion T, Vega S. 1992. A simple magic angle spinning NMR experiment for the dephasing of rotational echoes of dipolar coupled homonuclear spin pairs. Chem Phys Lett 194:423–428.
30. Ishii YJ. 2001. 13C–13C dipolar recoupling under very fast magic angle spinning in solid-state nuclear magnetic resonance: applications to distance measurements, spectral assignments, and high-throughput secondary-structure determination. J Chem Phys 114:8473–8483.
31. Bennett AE, Rienstra CM, Griffiths JM, Zhen WG, Lansbury PT, Griffin RG. 1998. Homonuclear radio frequency-driven recoupling in rotating solid. J Chem Phys 1998;108:9463–9479.
32. Oyler NA, Tycko R. 2002. Multiple quantum 13C NMR spectroscopy in solids under high-speed magic-angle spinning. J Phys Chem B 106:8382–8389.
33. Ishii Y, Balbach JJ, Tycko R. 2001. Measurement of dipole-coupled lineshapes in a many-spin system by constant-time two-dimensional solid state NMR with high-speed magic-angle spinning. Chem Phys 266:231–236.
34. Tycko R. 2004. Sensitivity enhancement in two-dimensional solid state NMR spectroscopy by transverse mixing. ChemPhysChem 5:863–868.
35. Chandrasekha S. 1992. Liquid Crystals, 2nd ed. Cambridge: Cambridge University Press.
36. Dong RY. 2010. Nuclear Magnetic Resonance Spectroscopy of Liquid Crystals. Singapore: World Scentific Publishing Co. Pte. Ltd.
37. Burnell EE, Langue CA, Meerts WL. 2010. Novel strategies for solving highly complex NMR spectra of solutes in liquid crystals. In: Ronald YD, ed. Nuclear Magnetic Spectroscopy of Liquid Crystals. Singapore: World Scientific Publishing, Co. Pte. Ltd.;1–35.
38. Weitekamp DP. 1983. Time-domain multiple-quantum NMR. Adv Magn Reson 11:111–274.
39. Rendell JCT. 1987. Multiple quantum NMR studies of solutes in liquid crystals. PhD Thesis, University of British Columbia.
40. Field LW, Terry ML.1986. Multiple-quantum NMR spectroscopy of molecules aligned in liquid crystal solvents. Selective quadrature detection of multiple-quantum spectra. J Magn Reson 69:176–179.
41. Rendell JCT, Burnell EE. 1995. Frequency selective excitation in multiple quantum NMR. J Magn Reson A 112:1–6.
42. Rendell JCT, Burnell EE. 1997. Analysis of single and multiple quantum NMR spectra of 1,3-dichloro-2-ethenylbenzene in liquid crystal solvents. In: Gielen M, Willem R, Wrackmeyer B, eds. Mol Phys 90:541–551.
43. Chandrakumar T, Polson JM, Burnell EE. 1996. A multiple-quantum 1H-NMR study of conformational biasing of biphenyl in a nematic liquid crystal. J Magn Reson A 118:264–271.

44. Stephenson DS, Binsch G. 1980. Automated analysis of high resolution NMR spectra. II. Illustrative applications of the computer program DAVINS. J Magn Reson 37:409–430.
45. Castiglione F, Celebre G, De Luca G, Longeri M. 2000. The NMR spectra of samples dissolved in liquid crystalline phases: automatic analysis with the aid of multiple quantum spectra—the case of flexible molecules. J Magn Reson 142:216–228.
46. Inoue K, Takeuchi H, Konaca S. 2001. Molecular structures of related compounds of mesogens studied by 1H NMR using a liquid crystal solvent: Tolan and trans-Azobenzene. J Phys Chem A 105:6711–6716.
47. Leo Meerts W, de Lange CA, Weber ACJ, Burnell EE. 2007. A simple two-step automatic assignment procedure for complicated NMR spectra of solutes in liquid crystals using genetic algorithms. Chem Phys Lett 441:342–346.
48. Rechenberg I. 1973. Evolutions strategie—Optimierung technischer Systeme nach Prinzipien der biologischen Evolution. Stuttgart, Germany: Frommann-Holzboog.
49. Hansen N, Ostermeier A. 2001. Completely derandomized self-adaptation in evolution strategies. Evol Comput 9:159–195.
50. Neuhaus D, Williamson MP. 2000. The Nuclear Overhauser Effect in Structural and Conformational Analysis, 2nd ed. New York: Wiley-VCH.
51. Butts CP, Jones CM, Towers EM, Flynn JL, Appleby L, Barron NJ. 2011. Interproton distance determinations by NOE—surprising accuracy and precision in a rigid organic molecule. Org Biomol Chem 9:177–184.
52. Williamson MP. 2009. Applications of NOE in molecular biology. In: Webb, GA, ed. Annual Reports on NMR Spectroscopy. Amsterdam: Elsevier. pp 77–109.
53. Clore GM, Gronenborn AM. 1998. New methods of structure refinement for macromolecular structure determination by NMR. Proc Natl Acad Sci USA 95: 5891–5898.
54. Clore GM, Robien MA, Gronenborn AM. 1993. Exploring the limits of precision and accuracy of protein structures determined by nuclear magnetic resonance spectroscopy. J Mol Biol 231:82–102.
55. Berman H. 2008. The Protein Data Bank: a historical perspective. Acta Crystallogr Sect A 64:88–95.
56. Rieping WH, Habeck M, Bardiaux B, Bernard A, Malliavin, Thérèse E, Nilges M. 2007. ARIA2: automated NOE assignment and data integration in NMR structure calculation. Bioinformatics 23:381–382.
57. Nabuurs SB, Spronk CAEM, Vriend G, Vuiste GW. 2004. Concepts and tools for NMR restraint analysis and validation. Concepts Magn Reson A 22:90–105.
58. Facelli JC. 2007. Calculation of chemical shieldings: theory and application. Concepts Magn Reson A 20: 42–69.
59. Contreras RH, Peralta JE, Giribet CG, Ruiz De Azua MC, Facelli JC. 2000. Advances in theoretical and physical aspects of spin-spin coupling constants. Annu Rep NMR Spectrosc 41:55–184.
60. Facelli JC. 2011. Chemical shift tensors: theory and application to molecular structural problems. Prog Nucl Magn Reson Spectrosc 58:176–201.
61. Andrew ER, Bradbury A, Eades RG, Jenks GJ. 1960. Fine structure of the nuclear magnetic resonances spectra of solids. Chemical shift structure of the spectrum of phosphorous pentachloride. Nature 188:1096–1097.
62. Andrew ER. 1981. Magic angle spinning in solid state NMR spectroscopy. Phil Trans Roy Soc London Ser A 299:505–520.
63. Kroto HW, Klein SI, Meidine MR, Nixon, JF, Harris RK, Packer KJ, Reams P. 1985. n1- and n2-Coordination in phosphaalkeneplatinum(0) complexes. High resolution solid state 31P NMR spectrum of mesityl(diphenylmethylene)phosphinebis-(triphenylphosphine)platinum(0). J Organomet Chem 280:281–287.
64. Gu Z, McDermott A. 1993. Chemical shielding anisotropy of protonated and deprotonated carboxylates in amino acids. J Am Chem Soc 115:4282–4285.
65. Solum MS, Altman KL, Strohmeier M, Berges DA, Zhang Y, Facelli JC, Pugmire RJ, Grant DM. 1997. 15N Chemical shift principal values in nitrogen heterocycles. J Am Chem Soc 119:9804–9809.
66. Pople JA, Beveridge DL. 1970. Approximate Molecular Orbital Theory. New York: McGraw-Hill.
67. Muller N, Pritchard DE. 1959. C-13 splittings in proton magnetic resonance spectra. I. Hydrocarbons. J Chem Phys 31:768–771.
68. Zhan C, Hu Z. 1993. Maximum bond order hybrid orbitals. I. Theoretical method. Theor Chim Acta 84: 511–520.
69. Kovaček D, Maksic ZB, Elbel S, Kudnig J. 1994. Semiempirical calculation of 29Si NMR chemical shifts and 29Si-13C spin–spin coupling constants in some substituted bridgehead polycycloalkanes. J Mol Struct (Theochem) 304:247–254.
70. Contreras RH, Aucar GA, Ruiz de Azua MC, Giribet CG. 1993. Theoretical analysis of NMR spin-spin coupling constants. Folia Chim Theor Latina 21:83–102.
71. Contreras RH, Natiello MA, Scuseria GE. 1985. Mechanisms which produce spin-spin coupling in NMR. Magn Reson Rev 9:239–321.
72. Contreras RH, Peralta JE. 2000. Angular dependence of spin-spin coupling constants. Prog Nucl Magn Reson Spectrosc 37:321–425.
73. Elyashber ME, Blinov KA, Williams AJ. 2009. The application of empirical methods of ^{13}C NMR chemical shift prediction as a filter for determining possible relative stereochemistry. Magn Reson Chem 47:333–341.
74. Bremser W. 1978. HOSE-a novel substructure code. Anal Chim Acta 103:355–365.
75. Jameson CJ, de Dios AC. 1993. The nuclear shielding surface: the shielding as a function of molecular geometry and intermolecular separation. In: Tossell JA, ed. Nuclear

Magnetic Shieldings and Molecular Structures. Dordrecht: Kluwer Academic Publishers. pp 95–116.
76. de Dios AC, Jameson CJ. 1994. The NMR chemical shifts: insight into structure and enviroment. Annu Rep NMR Spectrosc 29:1–69.
77. Wasylishen RE, Friedrich JO, Mooibroek S, Macdonald JB. 1985. Isotope shifts and spin-spin coupling constants in the carbon-13 and oxygen-17 NMR spectra of carbon monoxide and carbon dioxide. J Chem Phys 83:548–551.
78. Jameson CJ. 1996. Isotope effects on chemical shifts and coupling constants. In: Grant DM, Harris RK, eds. Encyclopedia of Magnetic Resonance. London: Wiley; 2638–2655.
79. Chesnut DB, Wright DW. 1991. Chemical shift bond derivatives for molecules containing first-row elements. J Comput Chem 12:546–559.
80. de Dios AC, Pearson JG, Oldfield E. 1993. Chemical shift in proteins: an ab intio study of carbon-13 nuclear magnetic resonance chemical shielding in glycine, alanine, and valine residues. J Am Chem Soc 115:9768–9773.
81. Iuliucci RJ, Phung Cu G, Facelli JC, Grant DM. 1996. Carbon-13 chemical shift tensors in polycyclic aromatic compounds. 6. single-crystal study of perylene. J Am Chem Soc 118:4880–4888.
82. Grant DM, Liu F, Iuliucci, Robbie J, Phung Cu G, Facelli JC, Alderman DW. 1995. Relationship of ^{13}C NMR chemical shift tensors to diffraction structures. Acta Crystallogr B 51:540–546.
83. Liu F, Orendt AM, Alderman DW, Grant D. 1997. Carbon-13 chemical shift tensors in pentaerythritol. J Am Chem Soc 119:8981–8984.
84. Grant DM, Halling MD. 2009. Metric spaces in NMR crystallography. Concepts Magn Reson A 34:217–237.
85. Facelli JC, Orendt AM, Grant DM, Michl J. 1984. IGLO calculations of the antisymmetric components of nuclear magnetic shielding tensors. Chem Phys Lett 112:147–149.
86. Facelli JC, Grant DM. 1993. Determination of molecular symmetry in crystalline naphthalene using solid-state NMR. Nature (London, United Kingdom) 365:325–327.
87. Facelli JC, Contreras RH, Scuseria GE, Engelmann AR. 1979. The contribution of molecular vibrations to calculated spin-spin coupling constants: a comparison of different commonly used methods. J Mol Struct 57:299–303.
88. Facelli JC, Orendt AM, Beeler AJ, Solum MS, Depke G, Malsch KD, Downing JW, Murthy PS, Grant DM, Michl J. 1985. Low-temperature carbon-13 magnetic resonance in solids. V. Chemical shielding anisotropy of the 13CH2 group. J Am Chem Soc 107:6749–6754.
89. Vanderhart DL. 1976. Characterization of the methylene 13C chemical shift tensor in the normal alkane *n*-C20H42. J Chem Phys 64:830.
90. Jameson CJ, de Dios AC. 2007. Theoretical and physical aspects of nuclear shielding. In: Webb GA, ed. Specialist Periodical Reports on Nuclear Magnetic Resonance. London: Royal Society. pp 50–71.
91. Jameson CJ, de Dios AC. 2009. Theoretical and physical aspects of nuclear shielding. In: Webb GA, ed. Nuclear Magnetic Resonance. London: The Royal Soc. pp 68–93.
92. Paul EG, Grant DM. 1963. Additivity relationships in carbon-13 chemical shift data for the linear alkanes. J Am Chem Soc 85:1701–1702.
93. Bunn A, Cudby MAE, Harris RK, Packer KJ, Say BJ. 1981. Solid-state high-resolution 13C NMR spectra of polypropene. J Chem Soc Chem Commun 1981:15.
94. Solum MS, Facelli, JC, Michl J, Grant D. 1986. Low-temperature carbon-13 magnetic resonance in solids. VII. Methyl carbons. J Am Chem Soc 108:6464–6470.
95. Facelli JC, et al. 1996. Carbon-13 chemical shift tensors and molecular conformation of anisole. J Phys Chem 100:8268–8272.
96. Carter CM, et al. 1988. Carbon-13 chemical-shift tensors in single-crystal methoxybenzenes. J Chem Soc Faraday Trans 1 84:3673–3690.
97. Harper JK, Arif AM, Grant DM. 2000. *Cis*-Verbenol. Acta Crystallogr C 56:451–452.
98. Harper JK, et al. 2002. 13C NMR Investigation of solid-state polymorphism in 10-deacetyl baccatin III. J Am Chem Soc 124:10589–10595.
99. Harper JK, et al. 2003. Stereochemical analysis by solid-state NMR: structural predictions in ambuic acid. J Org Chem 68:4609–4614.
100. Smith J, et al. 1998. Application of two-dimensional 13C solid-state NMR to the study of conformational polymorphism. J Am Chem Soc 120:11710–11713.
101. Smith JR, Xu W, Raftery D. 2006. Analysis of conformational polymorphism in pharmacuetical solids using solid state NMR and electronic structure calculations. J Phys Chem B 110:7766–7776.
102. Harris RK, et al. 2007. NMR crystallography of oxybuprocaine hydrochloride, modification II. Phys Chem Chem Phys 9:360–368.
103. de Dios AC, Oldfield E. 1994. Chemical shifts of carbonyl carbons in peptides and proteins. J Am Chem Soc 116:11485–11488.
104. de Dios AC, Oldfield E. 1996. Recent progress in understanding chemical shifts. Solid State Nucl Magn Reson 6:101–125.
105. Shen Y, Bax A. 2007. Protein backbone chemical shifts predicted from searching a database for torsion angle and sequence homology. J Biomol NMR 38:289–302.
106. Aguilar-Parrilla F, et al. 1994. 15N NMR chemical shifts of NH-pyrazoles in the solid state and in solution at low temperature. Magn Reson Chem 32:699–702.
107. Wishart DS, Sykes BD, Richards FM. 1991. Relationship between nuclear magnetic resonance chemical shift and protein secondary structure. J Mol Biol 222:311–333.
108. Neal S, et al. 2006. Accurate prediction of protein torsion angles using chemical shifts and sequence homology. Magn Reson Chem 44:S158–S167.

109. Vila JA, Ripoll DR, Scheraga HA. 2007. Use of 13C—a chemical shifts in protein structure determination. J Phys Chem B 111:6577–6585.
110. de Dios AC, Pearson JG, Oldfield E. 1993. Secondary and tertiary structural effects on protein NMR chemical shifts: an ab initio approach. Science (Washington, DC, United States) 260:1491–1496.
111. de Dios AC, Oldfield E. 1994. Ab initio study of the effects of torsion angles on carbon-13 nuclear magnetic resonance chemical shielding in *N*-formyl-L-alanine amide, *N*-formyl-L-valine amide, and some simple model compounds: applications to protein NMR spectroscopy. J Am Chem Soc 116:5307–5314.
112. Havlin R, et al. 1997. Solid state NMR and density functional investigations of carbon-13 shielding tensors in metal–olefin complexes. J Phys Chem A 101:8908–8913.
113. Heller J, et al. 1997. Determination of dihedral angles in peptides through experimental and theoretical studies of α-carbon chemical shielding tensors. J Am Chem Soc 119:7827–7831.
114. Matsunaga N, Sohlberg K. 2002. The effect of substituents on molecular electronic junctions. J Nanosci Nanotechnol 2:659–667.
115. Strohmeier M, Grant DM. 2004. Experimental and theoretical investigation of the 13C and 15N chemical shift tensors in melanostatin-exploring the chemical shift tensor as a structural probe. J Am Chem Soc 126:966–977.
116. Xu XP, Au-Yeung SCF. 2000. Investigation of chemical shift and structure relationships in nucleic acids using NMR and density functional theory methods. J Phys Chem B 104:5641–5650.
117. Precechtelova H, et al. 2007. Relationships between 31P chemical shifts tensors and conformation of nucleic acid backbone: a DFT study. J Phys Chem B 111:2658–2667.
118. Ghose R, et al. 1994. Dependence of 13C chemical shifts on glycosidic torsional angles in ribonucleic acids. J Am Chem Soc 116:8827–8828.
119. Ebrahimi M, et al. 2001. Dependence of 13C NMR chemical shifts on conformations of RNA nucleosides and nucleotides. J Magn Reson 150:1–9.
120. Saito H. 1996. Polysaccharide solid state NMR. In: Grant DM, Harris RK, eds. Encyclopedia of Magnetic Resonance. London: Wiley; 3740–3745.
121. Sergeyev I, Moyna G. 2005. Determination of the three dimensional structure of oligosaccharides in the solid state from experimental 13C NMR data and ab initio chemical shift surfaces. Carbohydr Res 340:1165–1174.
122. NIST Standard Reference Database, C.C.C.a.B.D. 2004.
123. Karplus M. 1959. Contact electron-spin coupling of nuclear magnetic moments. J Chem Phys 30:11–15.
124. Haasnoot CAG, De Leeuw FAAM, Altona C. 1980. The relation between proton-proton NMR coupling constants and substituent electronegativities. I. An empirical generalization of the Karplus equation. Tetrahedron 36:2783–2792.
125. Parr WJE, Schaefer T. 1980. The J method: application of NMR spectroscopy to the determination of small internal rotation barriers in solution. Acc Chem Res 13:400–406.
126. San Fabián J, et al. 1993. Chem Phys Lett 206:253.
127. San Fabián J, et al. 1994. Vicinal proton-proton coupling constants. IV. Effect of individual substituents with second row α-atoms. Mol Phys 82:913–928.
128. Guilleme J, San Fabian J, Diez E. 1997. Vicinal proton–proton coupling constants. V. Couplings to methyl groups. Mol Phys 91:343–356.
129. San Fabián J, Guilleme J, Diez E. 1995. Effect of b hydrogens on vicinal proton couplings 3JHH. Anal Quim 91:200–205.
130. Schaefer T, et al. 1994. A precise analysis of the 1H nuclear magnetic resonance spectrum of 2-phenyl-1,3-dithiane. Ring pucker, signs of long-range J(H,H), internal rotational barrier, and van der Waals shifts. Can J Chem 72:1722–1727.
131. Barfield M, Smith WB. 1992. Internal H-C-C angle dependence of vicinal 1H-1H coupling constants. J Am Chem Soc 114:1574–81.
132. Smith WB, Barfield M. 1993. Predictions of 3J(HH) near 180°—reparameterization of the sp3—sp3 equation. Magn Reson Chem 31:696–697.
133. Vuister GW, Bax A. 1993. Quantitative J correlation: a new approach for measuring homonuclear three-bond J(HNHa) coupling constants in 15N-enriched proteins. J Am Chem Soc 115:7772–7777.
134. Jimeno M, et al. 1996. 1H NMR study of the conformation of metallapentacycles NCCOM [M = Rh(III) and Ir(III)] resulting in a Karplus-type relationship for vicinal H-C(sp3)-N(sp3)-H coupling constants. Magn Reson Chem 34:42–46.
135. Engelsen SB, et al. 1995. Internal motions of carbohydrates as probed by comparative molecular modeling and nuclear magnetic resonance of ethyl β-lactoside. J Comput Chem 16:1096–1119.
136. Altona C, et al. 1994. Empirical group electronegativities for vicinal NMR proton-proton couplings along a C-C bond: solvent effects and reparameterization of the Haasnoot equation. Magn Reson Chem 32:670–678.
137. Tvaroska I, Hricovini M, Petrakova E. 1989. An attempt to derive a new Karplus-type equation of vicinal proton-carbon coupling constants for C-O-C-H segments of bonded atoms. Carbohydr Res 189:359–362.
138. Rundlof T, et al. 1998. Long-range proton-carbon coupling constants in conformational analysis of oligosaccharides. Magn Reson Chem 36:839–847.
139. San Fabián J, Guilleme J, Diez E. 1998. Vicinal carbon-proton coupling constants. Angular dependence and fluorine substituent effects. Theochem 426:117–133.
140. Wang AC, Bax A. 1995. Reparametrization of the Karplus relation for 3J(Ha-N) and 3J(HN-C') in peptides from uniformly 13C/15N-enriched human ubiquitin. J Am Chem Soc 117:1810–1813.
141. Wang AC, Bax A. 1996. Determination of the backbone dihedral angles j in human ubiquitin from

reparametrized empirical karplus equations. J Am Chem Soc 118:2483–2494.
142. Parella T, Sanchez-Ferrando F, Virgili A. 1997. Experimental evidence for the breakdown of the Karplus relationship for 3J(13C, 1H) in 1H-C-C=13C Systems. Magn Reson Chem 35:30–34.
143. Keah HH, Rae ID. 1993. Vicinal carbon-hydrogen coupling as an aid to stereochemical assignments in substituted propenoic acids. Aust J Chem 46:1413–1419.
144. Marton J, et al. 1996. Morphine alkaloids. 134. Reaction of morphinan-6,8-dienes with azadienophiles. Tetrahedron 52:2449–2464.
145. Orendt AM. 2003. Chemical shift tensor measurement in solids. In: Grant DM, Harris RK, eds. Encyclopedia of Nuclear Magnetic Resonance. London: Wiley. pp 1282–1296.
146. Orendt AM, Facelli JC. 2007. Solid state effects on NMR chemical shifts. Ann Rep NMR Spectrosc 62: 115–178.
147. Augspurger JD, et al. 1993. Intra - and intromolecular electrial effects on nuclear magnetic resonance, nuclear quadrupole resonance and infra-red pectroscopic parameters from ab initio calculation and experiment: from CO to proteins. In: Tossell JA, ed. Nuclear Magnetic Shieldings and Molecular Structure, Vol. 386. Boston: Kluwer Academic Publisher.
148. de Dios AC, Oldfield E. 1993. Methods for computing nuclear magnetic resonance chemical shielding in large systems. Multiple cluster and charge field approaches. Chem Phys Lett 205:108–116.
149. Ferraro MB, Repetto V, Facelli JC. 1998. Modeling NMR chemical shifts: a comparison of charge models for solid state effects on 15N chemical shift tensors. Solid State Nucl Magn Reson 10: 185–189.
150. Solis D, Ferraro MB. 2000. Solid-state nuclear magnetic resonance: performance of point-charge distributions to model intermolecular effects in 19F chemical shifts. Theor Chem Acc 104:323–326.
151. Solis D, Ferraro MB, Facelli JC. 2002. Modeling NMR chemical shifts: surface charge representation of the electrostatic embedding potential modeling of crystalline intermolecular effects in 19F solid state NMR chemical shifts. J Mol Struct 602–603:159–164.
152. Stueber D, Guenneau FN, Grant DM. 2001. The calculation of 13C chemical shielding tensors in ionic compounds utilizing point charge arrays obtained from Ewald lattice sums. J Chem Phys 114:9236–9243.
153. Stueber D, et al. 2002. Carbonates, thiocarbonates, and the corresponding monoalkyl derivatives. III.1. The 13C chemical shift tensors in potassium carbonate, bicarbonate and related monomethyl derivatives. Solid State Nucl Magn Reson 22:29–49.
154. Di Fiori N, et al. 2004. Modeling solid state effects on NMR chemical shifts using electrostatic models. Magn Reson Chem 42:S41–S47.
155. von Ragué Schleyer P, et al. 1996. Nucleus-independent chemical shifts: a simple and efficient aromaticity probe. J Am Chem Soc 118:6317–6318.
156. Jemmis ED, et al. 1997. The remarkably stabilized trilithiocyclopropenium ion, C3Li3+, and its relatives. J Am Chem Soc 119:9504–9512.
157. Jiao H, et al. 1998. Theoretical studies of the structure, aromaticity, and magnetic properties of o-benzyne. Angew Chem Int Ed 36:2761–2764.
158. Facelli JC. 2006. Intermolecular shielding by molecular magnetic susceptibility. A new view of intermolecular ring current effects. Magn Reson Chem 44:401–408.
159. Sebastiani D, Parrinello M. 2001. A new ab-initio approach for the calculation of NMR chemical shifts in periodic systems. J Phys Chem A 105:1951–1958.
160. Sebastiani D, et al. 2002. NMR chemical shifts in periodic systems from first principles. Comput Phys Commun 147:707–710.
161. Sebastiani D. 2003. Ab-Initio calculations of NMR parameters in condensed phases. Mod Phys Lett B 17:1301–1319.
162. Sebastiani D, Rothlisberger U. 2004. Nuclear magnetic resoance chemical shifts from hybrid DFT QM/MM calculations. J Phys Chem B 108:2807–2815.
163. Sebastiani D. 2006. Current densities and nucleus-independent chemical shift maps from reciprocal-space density functional perturbation theory calculations. ChemPhysChem 7:164–175.
164. Parrinello M, Andreoni A. CPMD V3.9, http://www.cpmd.org/. Copyright IBM Corp 1990–2006, Copyright MPI fuer Festkoerperforschung Stuttgart, 1997–2001.
165. Mauri F, Pfrommer BG, Louie SG. 1996. Ab initio theory of NMR chemical shifts in solids and liquids. Phys Rev Lett 77:5300–5303.
166. Pickard CJ, Mauri F. 2001. All-electron magnetic response with pseudopotentials: NMR chemical shifts. Phys Rev B 63:245101.
167. Gregor T, Mauri F, Car R. 1999. A comparison of methods for the calculation of NMR chemical shifts. J Chem Phys 111:1815–1822.
168. Buda F, Giannozzi P, Mauri F. 2000. Density functional theory study of the structure and ^{13}C chemical shifts of retinylidene iminium salts. J Phys Chem B 104:9048–9053.
169. Pfrommer BG, Mauri F, Louie SG. 2000. NMR chemical shifts of ice and liquid water: the effects of condensation. J Am Chem Soc 122:123–129.
170. Yates JR. et al. 2003. Relativistic nuclear magnetic resonance chemical shifts of heavy nuclei with pseudopotentials and the zeroth-order regular approximation. J Chem Phys 118:5746–5753.
171. Gervais C, et al. 2005. Combined first-principles computational and experimental multinuclear solid-state NMR investigation of amino acids. J Phys Chem A 109:6960–6969.

172. Yates JR, et al. 2004. Theoretical investigation of oxygen-17 NMR shielding and electric field gradients in glutamic acid polymorphs. J Phys Chem A 108:6032–6037.
173. Benoit M, et al. 2005. First-principles calculation of the ^{17}O NMR parameters of a calcium aluminosilicate glass. J Phys Chem B 109:6052–6060.
174. Rossano S, et al. 2005. First-principles calculation of ^{17}O and ^{25}Mg NMR shieldings in MgO at finite temperature: rovibrational effect in solids. J Phys Chem B 109:7245–7250.
175. Yates JR, et al. 2005. A combined first principles computational and solid-state NMR study of a molecular crystal: flurbiprofen. Phys Chem Chem Phys 7:1402–1407.
176. Giannozzi P, et al. 2009. QUANTUM ESPRESSO: a modular and open-source software project for quantum simulations of materials. J Phys Condens Matter 21:395502–395519.
177. Harris KDM. 2003. New oportunities for structure determination of molecular materials directly from powder diffraction data. Cryst Growth Des 3:887–895.
178. Harris KDM, Xu M. 2009. Combined analysis of NMR & powder diffraction data. In: Harris RK, Wasylishen RE, Duer MJ, eds. NMR Crystallography. London: Wiley. pp 275–286.
179. Harris RK, Wasylishen RE, Duer MJ. 2009. NMR Crystallography. London: Wiley.
180. Meejoo S, et al. 2003. Structural aspects of the β-polymorph of (*E*)−4-formylcinnamic acid: structure determination directly from powder diffraction data and elucidation of structural disorder from solid-state NMR. Helv Chim Acta 86:1467–1477.
181. Witter R, et al. 2006. ^{13}C Chemical shift constrained crystal structure refinement of cellulose iα and its verification by NMR anisotropy experiments. Macromolecules 39:6125–6132.
182. Nishiyama Y, et al. 2003. Crystal structure and hydrogen bonding system in cellulose 1(α), from synchrotron X-ray and neutron fiber diffraction. J Am Chem Soc 125:14300–14306.
183. Harper JK, et al. 2010. A combined solid-state NMR and synchrotron X-ray diffraction powder study on the structure of the antioxidant (+)-Catechin 4.5-hydrate. J Am Chem Soc 132:2928–2937.
184. Heider EM, Harper JK, Grant DM. 2007. Structural characterization of an anhydrous polymorph of paclitaxel by solid-state NMR. Phys Chem Chem Phys 9:6083–6097.
185. Gervais C, et al. 2004. Ab initio calculations of NMR parameters of highly coordinated oxygen sites in aluminosilicates. J Phys Chem B 108:13249–13253.
186. Malkin VG, et al. 1994. Nuclear magnetic resonance shielding tensors calculated with a sum-over-states density functional perturbation theory. J Am Chem Soc 116:5898–5908.
187. Frisch MJ, et al. 2009. Gaussian 09, Revision A.1. Wallingford, CT: Gaussian, Inc.
188. Wolinski K, Hinton JF, Pulay P. 1990. Efficient implementation of the gauge-independent atomic orbital method for NMR chemical shift calculations. J Am Chem Soc 112:8251–8260.
189. Pulay P, Hinton JF. 1996. Shielding theory: GIAO method. In: Grant DM, Harris RK, eds. Encyclopedia of Nuclear Magnetic Resonance. London: Wiley. pp 4334–4339.
190. Hinton JF, et al. 1992. Ab initio quantum mechanical calculation of the chemical shift anisotropy of the hydrogen atom in the $(H_2O)_{17}$ cluster. J Am Chem Soc 114:1604–1605.

BIOGRAPHIES

Julio C. Facelli was born in Buenos Aires, Argentina and attended the University of Buenos Aires where he got his Ph.D. in physics in 1982. He is Professor and Vice Chair of the Department of Biomedical Informatics, Director of the Biomedical Informatics Core of the Center Clinical and Translation Sciences, Adjunct Professor of Chemistry and Physics and Faculty member of the Institute for Clean and Safe Energy and the Nano Utah Institute at the University of Utah. Dr. Facelli has been member of numerous University Committees dealing with Information Technology. Dr. Facelli is co-author of more than 180 international per review publications.

Marta B. Ferraro was born in Buenos Aires, Argentina. Marta B. Ferraro got her graduation degree, Licenciada en Física, from Facultad de Ciencias Exactas y Naturales (FCEN), Universidad de Buenos Aires (UBA), in 1977, and her Ph.D. from Universidad de Buenos Aires (UBA), in 1985, with supervision of Prof. R. H. Contreras. She became Professor at the Physics Department of FCEN, UBA in 1986, and researcher of Consejo Nacional de Investigaciones Científicas y Técnicas (CONICET) from 1989. Her group at Buenos Aires develops joint projects with Prof. J. C. Facelli at Utah University, and with Prof. S.P.A. Sauer at Copenhagen University. MBF current research focuses on analysis of high resolution NMR parameters and their relation with structures, NMR solid state, and prediction of structures and properties of pharmaceutical crystals. Dr. Ferraro has more than 90 per review publications.